

Title: NEON Imaging Spectrometer Radiance to Reflectance Algorithm Theoretical Basis Document		Date: 02/11/2015
NEON Doc. #: NEON.DOC.001288	Author: B. Karpowicz, T. Kampe	Revision: A

## NEON IMAGING SPECTROMETER RADIANCE TO REFLECTANCE ALGORITHM THEORETICAL DOCUMENT

PREPARED BY	ORGANIZATION	DATE
Bryan Karpowicz	AOP	08/01/2013
Thomas Kampe	AOP	10/08/2014

APPROVALS	ORGANIZATION	APPROVAL DATE
Hanne Buur	PSE	02/05/2015
Shelley Petroy	DPS	01/08/2015

RELEASED BY	ORGANIZATION	RELEASE DATE
Judy Salazar	CM	02/11/2015

See configuration management system for approval history.



<i>Title:</i> NEON Imaging Spectrometer Radiance to Reflectance Algorithm Theoretical Basis Document		<i>Date:</i> 02/11/2015
<i>NEON Doc. #:</i> NEON.DOC.001288	<i>Author:</i> B. Karpowicz, T. Kampe	<i>Revision:</i> A

The National Ecological Observatory Network is a project solely funded by the National Science Foundation and managed under cooperative agreement by NEON, Inc. Any opinions, findings, and conclusions or recommendations expressed in this material are those of the author(s) and do not necessarily reflect the views of the National Science Foundation.

### Change Record

REVISION	DATE	ECO #	DESCRIPTION OF CHANGE
A	02/11/2015	ECO-02608	Initial release

Title: NEON Imaging Spectrometer Radiance to Reflectance Algorithm Theoretical Basis Document		Date: 02/11/2015
NEON Doc. #: NEON.DOC.001288	Author: B. Karpowicz, T. Kampe	Revision: A

**TABLE OF CONTENTS**

**1 DESCRIPTION.....1**

1.1 Purpose ..... 3

1.2 Scope..... 3

**2 RELATED DOCUMENTS AND ACRONYMS .....3**

2.1 Applicable Documents ..... 3

2.2 Reference Documents..... 3

2.3 External References ..... 4

2.4 Acronyms ..... 4

**3 DATA PRODUCT DESCRIPTION.....5**

3.1 Variables Reported ..... 6

3.2 Input Dependencies ..... 8

3.3 Product Instances, Temporal/Spatial Resolution and Extent ..... 10

3.3.1 Temporal Resolution and Extent..... 11

3.3.2 Spatial Resolution and Extent ..... 11

**4 SCIENTIFIC CONTENT .....12**

4.1 Theory of Measurement/Observation..... 12

4.2 Theory of the Algorithm..... 13

**5 ALGORITHM IMPLEMENTATION.....13**

5.1 Atmospheric Transmission Computation..... 15

5.2 Extraterrestrial Solar Irradiance Curve Source ..... 16

5.3 Aerosol Retrieval..... 16

5.4 Water Vapor Retrieval ..... 19

5.5 BRDF Correction..... 21

5.5.1 Nadir Normalization Method ..... 21

5.5.2 Empirical BRDF in Rugged Terrain..... 22

5.6 Haze Removal..... 23

5.7 Cloud Shadow Removal ..... 24

5.8 Adjacency Effect Correction..... 29

5.8.1 Atmospheric Correction with Adjacency Effect assuming Flat Terrain..... 29

Title: NEON Imaging Spectrometer Radiance to Reflectance Algorithm Theoretical Basis Document		Date: 02/11/2015
NEON Doc. #: NEON.DOC.001288	Author: B. Karpowicz, T. Kampe	Revision: A

5.8.2	Atmospheric Correction assuming Rugged Terrain .....	36
<b>6</b>	<b>UNCERTAINTY .....</b>	<b>38</b>
6.1	Analysis of Uncertainty .....	40
6.2	Reported uncertainty.....	40
<b>7</b>	<b>VALIDATION AND VERIFICATION .....</b>	<b>41</b>
<b>8</b>	<b>FUTURE MODIFICATIONS AND PLANS.....</b>	<b>41</b>
<b>9</b>	<b>BIBLIOGRAPHY .....</b>	<b>41</b>

**LIST OF TABLES AND FIGURES**

Table 1: Variables Reported.....	8
Table 2: Input Dependencies .....	9
Table 3: Symbols and Notation.....	9
Table 4: Instance, Temporal/Spatial Resolution and Extent.....	10
Table 5: ATCOR spectral sampling in monochromatic database.....	16
Table 6. Initial NIS Radiance to Reflectance Retrieval Error Tree.....	39

Figure 1: A sample MODTRAN model of at-sensor radiance spectrum for the NIS showing major molecular absorption bands. ....	2
Figure 2: Variable/File Generation for ATCOR.....	6
Figure 3: Reflectance data product output file structure following atmospheric correction .....	7
Figure 4: Illustration of the atmospheric correction process.....	13
Figure 5: Atmospheric Correction Steps in ATCOR.....	15
Figure 6: Flowchart describing the cloud shadow removal process.....	28
Figure 7. Radiation components contributing to at-sensor radiance.....	29
Figure 8. Spectra of vegetation, soil and black tar background used in simulation. ....	30
Figure 9. Calculated spectral reflectance difference caused by adjacency effect for soil/tar background case. ....	31
Figure 10. Calculated reflectance difference caused by adjacency effect for vegetation/tar background case. ....	32
Figure 11: Atmospheric Correction with Rugged Terrain .....	36

Title: NEON Imaging Spectrometer Radiance to Reflectance Algorithm Theoretical Basis Document		Date: 02/11/2015
NEON Doc. #: NEON.DOC.001288	Author: B. Karpowicz, T. Kampe	Revision: A

**1 DESCRIPTION**

This document describes the algorithm for retrieving the Level 1 land surface reflectance data product from the NEON Imaging Spectrometer (NIS) Level 1 calibrated and geolocated radiance data product. The NIS is a Visible-to-Shortwave Infrared (VSWIR) imaging spectrometer operating in the solar spectral region between 0.38 and 2.5 microns with a spectral sampling of 0.5 nm. It is one of the primary instruments flown aboard the NEON Airborne Observation Platform (AOP) (RD [04]).

The radiances received by the NIS in the solar spectral region are affected by absorption and scattering from atmospheric gases and aerosols. In order for VSWIR data to be used for quantitative ecological studies of the Earth’s surface, these atmospheric effects need to be removed. To apply these measurements to quantitative scientific data products, it is necessary to convert the measured spectral radiance ( $L$ ) to surface reflectance, ( $\rho$ ). This is the focus of this algorithm, the third major processing step in the development of the NIS L-1 data products, as discussed in RD [05].

The conversion of radiance to reflectance involves a process known as atmospheric correction which accounts for the attenuation and scattering due to atmospheric constituents in a real atmosphere. One must account for aerosols (e.g., small particles such as mineral dust, smoke and soot particles, and industrial pollutants), water vapor, and other mixed gases across the spectral range of interest. The determination of other atmospheric characteristics, including molecular scattering and surface pressure, are also required.

The solar radiation along the Sun-Surface-Sensor path is subject to wavelength-dependent absorption and scattering by the atmosphere and surface. As shown in Figure 1, major water vapor absorption bands, centered at 940, 1140, 1380, and 1880 nm, are present within the NIS spectral region of interest (i.e., 380 – 2500 nm). In addition, gaseous absorption must also be accounted for, primarily due to the oxygen A-band absorption band at 760 nm and a strong carbon dioxide band near 2080 nm. At wavelengths shorter than 1000 nm, the measured radiance is also affected by molecular and aerosol scattering.

Accurate atmospheric correction is especially critical for NEON since the goal is to acquire spectroscopic data over a large number of sites (~100) distributed across the continental United States that will be affected by a broad range of atmospheric conditions. As an example, it can be anticipated that NEON remote sensing acquisitions will occur under conditions that can range from dry, clear conditions to dusty (i.e., in the desert Southwest) to humid conditions (Southeast U.S. in the summer months) to polluted conditions (East Coast summer). Therefore,

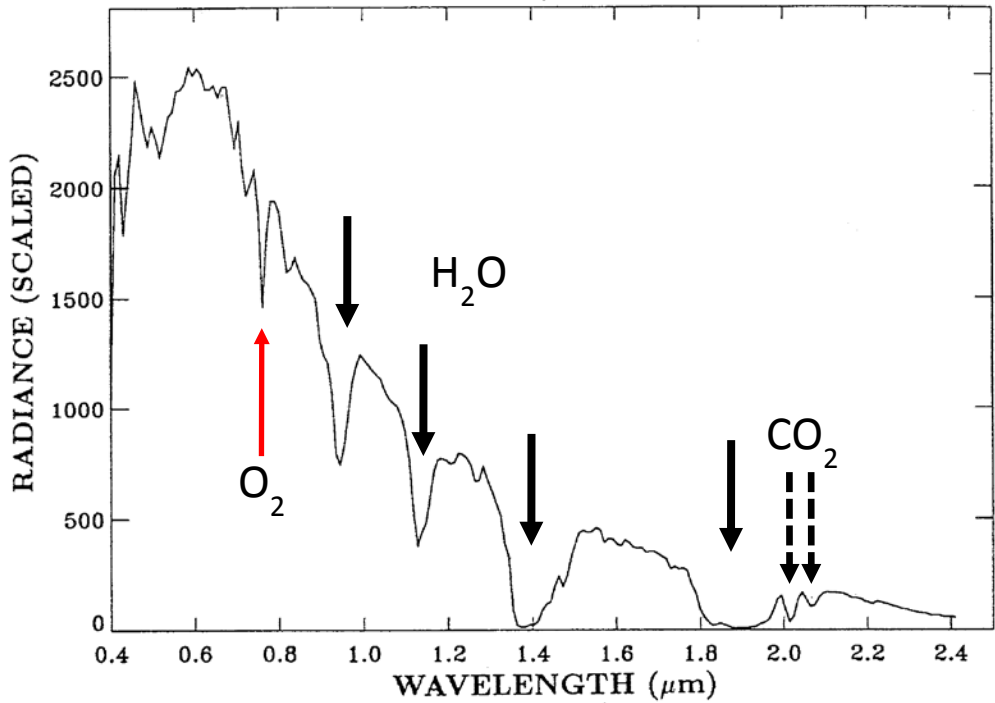


Figure 1: A sample MODTRAN model of at-sensor radiance spectrum for the NIS showing major molecular absorption bands.

the atmospheric correction algorithms employed by NEON must be robust over a range of conditions. The ability to determine the absolute reflectance without prior knowledge of surface characteristics and potentially atmospheric conditions at the time of acquisition requires the application of atmospheric radiative transfer modeling. This step in the surface reflectance retrieval has been identified as the largest source of error in deriving surface reflectance from imaging spectrometer data (Goetz *et al.*, 1998).

A number of radiative transfer atmospheric correction algorithms have been developed for retrieving surface reflectances from imaging spectrometers and are in use in the field (Gao *et al.*, 2009). These include the High-Accuracy Atmospheric Correction for Hyperspectral Data (HATCH) code developed at the University of Colorado (Qu *et al.*, 2003), the Fast Line-of-Sight Atmospheric Analysis of Spectral Hyper Cubes (FLAASH) MODTRAN-based algorithm (Adler-Golden *et al.*, 1999) developed jointly by the Air Force Phillips Laboratory and Spectral Sciences Corp., and the Atmospheric CORrection Now (ACORN) algorithm (Kruse, 2004). NEON is using the ATCOR-4 algorithm (ER [01]) for atmospheric correction since it has the capability to correct for the influence of terrain as well as radiation reflected from neighboring pixels that is scattered into the viewing direction of the pixel of interest (the “adjacency” effect).

Title: NEON Imaging Spectrometer Radiance to Reflectance Algorithm Theoretical Basis Document		Date: 02/11/2015
NEON Doc. #: NEON.DOC.001288	Author: B. Karpowicz, T. Kampe	Revision: A

**1.1 Purpose**

This document details the algorithms used for creating NEON Level 1 spectral reflectance data product NEON.DOM.SIT.DP1G.30002.001.001.001.001 from Level 1 radiance data from NEON.DOM.SIT.DP1G.30001.001.001.001.001 and ancillary data supplied by the imaging spectrometer geolocation algorithm (RD [06]). The algorithm described herein produces a surface reflectance value for each spectrometer spectral radiance value supplied by NEON.DOM.SIT.DP1G.30002.001.001.001.001. The goal of the algorithm is to mitigate the influence of the atmosphere (scattering, and absorption), and take the measured radiance value in  $\mu\text{W cm}^{-2} \text{sr}^{-1} \text{nm}^{-1}$ , and convert it to a normalized value (zero to 1.0) of reflectance. This document includes a detailed discussion of the measurement theory and implementation, appropriate theoretical background, data product provenance, quality assurance and control methods used, approximations and/or assumptions made, and a detailed exposition of uncertainty resulting in a cumulative reported uncertainty for this product.

**1.2 Scope**

This document describes the theoretical background and entire algorithmic process required to convert of the Level-1 NEON.DOM.SIT.DP1G.30001.001.001.001.001 radiance product to obtain the Level-1 reflectance product NEON.DOM.SIT.DP1G.30002.001.001.001.001. It does not provide computational implementation details, except for cases where these stem directly from algorithmic choices explained here.

**2 RELATED DOCUMENTS AND ACRONYMS**

**2.1 Applicable Documents**

Applicable documents contain information that shall be applied in the current document. Examples are higher level requirements documents, standards, rules and regulations.

AD [01]	NEON.DOC.000001	NEON Observatory Design (NOD) Requirements
AD [02]	NEON.DOC.005003	NEON Scientific Data Products Catalog
AD [03]	NEON.DOC.005004	NEON Level 1-3 Data Products Catalog
AD [04]	NEON.DOC.005005	NEON Level 0 Data Product Catalog

**2.2 Reference Documents**

Reference documents contain information complementing, explaining, detailing, or otherwise supporting the information included in the current document.

Title: NEON Imaging Spectrometer Radiance to Reflectance Algorithm Theoretical Basis Document		Date: 02/11/2015
NEON Doc. #: NEON.DOC.001288	Author: B. Karpowicz, T. Kampe	Revision: A

RD [01]	NEON.DOC.000008	NEON Acronym List
RD [02]	NEON.DOC.000243	NEON Glossary of Terms
RD [03]	NEON.DOC.001210	NEON Imaging Spectrometer (NIS) Level 1B Calibrated Radiance Algorithm Theoretical Basis Document
RD [04]	NEON.DOC.002236	AOP Overview Document
RD [05]	NEON.DOC.001289	NEON Imaging Spectrometer Level-1 Processing Overview Document
RD [06]	NEON.DOC.001290	Imaging Spectrometer L0 to L1 Geolocation Processing Algorithm Theoretical Basis Document
RD [07]	NEON.DOC.001292	NEON L0 to L1 Discrete Return Lidar Algorithm Theoretical Basis Document
RD [08]	NEON.DOC.015029	AOP Calibration and Validation Plan

### 2.3 External References

External references contain information pertinent to this document, but are not NEON configuration-controlled. Examples include manuals, brochures, technical notes, and external websites.

ER [01]	<a href="http://www.rese.ch/products/atcor/index.html">http://www.rese.ch/products/atcor/index.html</a>	ATCOR Atmospheric & Topographic Correction Models
ER [02]	<a href="http://modtran5.com/">http://modtran5.com/</a>	MODTRAN5 Atmospheric radiative transfer model
ER [03]	Richter, R., and D. Schläpfer, ATCOR-4 User Guide, Version 6.3.2, September 2014	

### 2.4 Acronyms

APDA	Atmospheric Precorrected Differential Absorption
ATCOR	Atmospheric & Topographic Correction
BIL	Bit Interleaved by Line
BRDF	Bidirectional Reflectance Distribution Function
BSQ	Band Sequential
ENVI	ENvironment for Visualizing Images
DEM	Digital Elevation Model
FWHM	Full width Half Maximum
IFOV	Instantaneous Field of View
LIRR	Linear Regression Ratio
NIS	Neon Imaging Spectrometer
NDVI	Normalized Difference Vegetation Index
MODIS	Moderate Resolution Imaging Spectroradiometer
MODTRAN	MODerate resolution atmospheric TRANsmission
SBET	Smoothed Best Estimate Trajectory
SWIR	Short Wave Infrared

Title: NEON Imaging Spectrometer Radiance to Reflectance Algorithm Theoretical Basis Document		Date: 02/11/2015
NEON Doc. #: NEON.DOC.001288	Author: B. Karpowicz, T. Kampe	Revision: A

### 3 DATA PRODUCT DESCRIPTION

The primary NEON data product produced is reflectance. Typically, reflectance is derived by compensating for the influence from the atmosphere solar illumination, sensor viewing angle, and terrain effects. The current atmospheric correction code ATCOR is a commercial product (ER [01]), and has no real transparency beyond what is published in the manual (*Richter and Schläpfer, 2011*). Given that it is a proprietary algorithm, no source code is available to streamline into the NEON AOP data flow. A wrapper has been written to package required input files for ATCOR, and compile them into a single per flight line HDF5 file<sup>1</sup>. This process is summarized in Figure 2.

---

<sup>1</sup> <http://www.hdfgroup.org/HDF5/> : HDF5 is a data model, library, and file format for storing and managing data. It supports an unlimited variety of datatypes, and is designed for flexible and efficient I/O and for high volume and complex data. HDF5 is portable and is extensible, allowing applications to evolve in their use of HDF5. The HDF5 Technology suite includes tools and applications for managing, manipulating, viewing, and analyzing data in the HDF5 format.

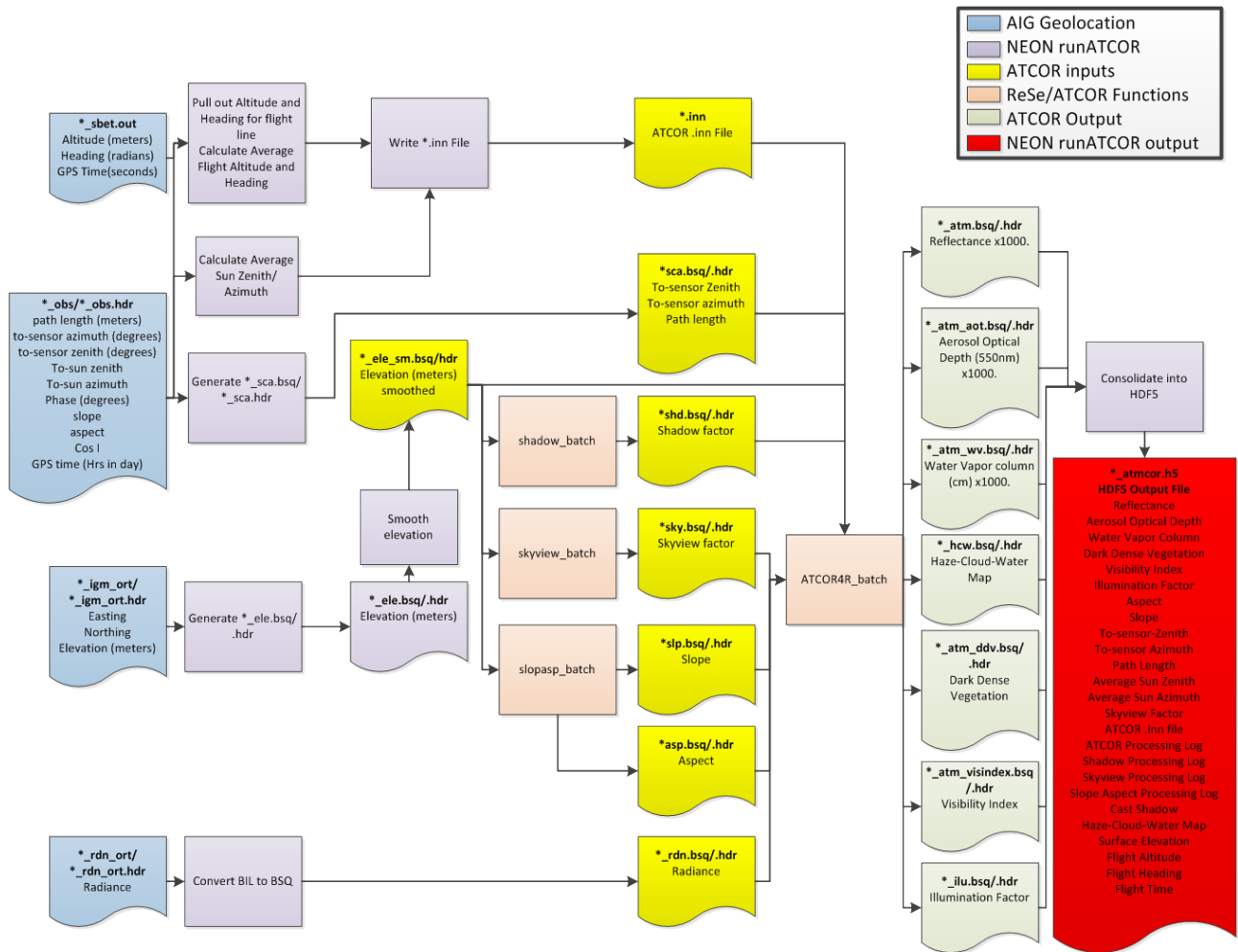


Figure 2: Variable/File Generation for ATCOR

### 3.1 Variables Reported

The reported variable from the atmospheric correction algorithm is the spectral reflectance. Reflectance is a normalized quantity (valid values between 0 and 1), and as a result has no units. The dimensions of the data will be by flight line (along-track dimension), spatial sample (cross-track dimension), and by band (wavelength dimension). Several additional variables are also reported as output from this algorithm and these are summarized in Table 1. The current output format is an HDF5 file (\*\_atmcor.h5). The structure of the output HDF5 file is presented in Figure 3.

Title: NEON Imaging Spectrometer Radiance to Reflectance Algorithm Theoretical Basis Document		Date: 02/11/2015
NEON Doc. #: NEON.DOC.001288	Author: B. Karpowicz, T. Kampe	Revision: A

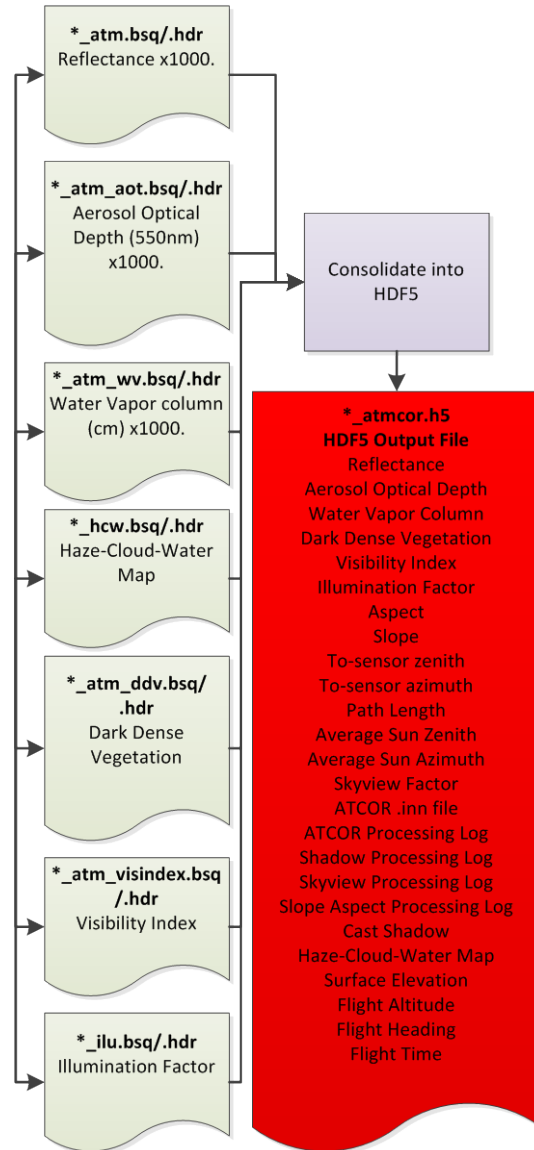


Figure 3: Reflectance data product output file structure following atmospheric correction

Table 1: Variables Reported

Variable Name	Description
Reflectance	Value from 0-1.0 indicating the reflectivity of surface at a given wavelength
Aerosol Optical Depth	Aerosol optical depth at 550 nm
Water Vapor Column	Total water vapor column reported in cm
Dark Dense Vegetation	Classification of regions which are considered dark enough for aerosol retrieval
Visibility Index	Visibility in km.
Illumination Factor	Intermediate product in terrain correction
Aspect	Aspect of the DEM after smoothing
Slope	Slope of the DEM after smoothing
To-Sensor Zenith	The to-sensor zenith angle from the platform
To-Sensor Azimuth	The to-sensor azimuth angle from the platform
Path Length	The distance from sensor to ground in meters
Average Sun Zenith	The solar zenith angle used in the ATCOR run
Average Sun Azimuth	The solar azimuth angle used in the ATCOR run
Sky View Factor	An intermediate product in the terrain correction
ATCOR .inn file	The input file for ATCOR
ATCOR Processing Log	The output processing log from ATCOR
Shadow Processing Log	The output from the shadow mask processing log
Skyview Processing Log	The output from skyview processing log
Slope/Aspect Processing Log	Slope/Aspect calculation processing log
Cast Shadow	Mask whether or not an object casts shadow
Haze-Cloud-Water Map	Map indicating regions of haze, cloud, or water bodies
Surface Elevation	The surface elevation used in ATCOR run
Flight Altitude	The altitude of the aircraft
Flight Heading	The recorded heading during the flight track
Flight Time	The time stamp of the flight track in GPS time (seconds of week UTC)

### 3.2 Input Dependencies

The input dependencies required for this algorithm are summarized in Table 2. The algorithm requires (1) the \*\_obs\_ort file (with its associated \*\_obs\_ort.hdr file) from the geolocation algorithm (RD [06]), (2) the \*\_rdn\_ort file (with its associated \*\_rdn\_ort.hdr file) from the radiance calibration algorithm (RD [03]), and (3) the SBET file from the trajectory calculation

Title: NEON Imaging Spectrometer Radiance to Reflectance Algorithm Theoretical Basis Document		Date: 02/11/2015
NEON Doc. #: NEON.DOC.001288	Author: B. Karpowicz, T. Kampe	Revision: A

(PosPac). Variables from the \*\_rdn\_ort file are radiance ( $\mu W cm^{-2} Sr^{-1} nm^{-1}$ ), wavelength (nm), and full width half maximum (FWHM). Variables from the \*\_obs\_ort file are Path Length (meters), To-sensor azimuth angle (degrees), To-sensor zenith angle (degrees), To-sun azimuth (degrees), To-sun zenith angle (degrees), Phase angle (degrees), Slope, Aspect, Cosine I, and GPS time (0-23 hours). In addition to the \*\_obs, and \*\_obs.hdr file, the atmospheric correction algorithm will require the surface elevation contained in the \*\_igm\_ort, and \*\_ort\_igm\_ort.hdr file. The SBET file contains a number of parameters including Heading (radians), flight altitude above sea level (meters), and the GPS time (seconds of week). Symbols and notations used in this document are presented in Table 3.

The current atmospheric correction program ATCOR (*Richter and Schläpfer, 2011*) requires the radiance data in BSQ (Band Sequential) format so that the \*\_rdn file must be converted to BSQ from BIL (Band Interleaved by Line) format. The required conversions of the input files to the files required by ATCOR are shown in Figure 2.

Table 2: Input Dependencies

Input Dependency	Source
Altitude (m)	SBET (trajectory)
Heading (radian)	SBET (trajectory)
GPS seconds (sec)	SBET (trajectory)
To-Sun Zenith (deg)	obs_ort (geolocation)
To-Sun Azimuth (deg)	obs_ort (geolocation)
To-Sensor Zenith (deg)	obs_ort (geolocation)
To-Sensor Azimuth (deg)	obs_ort (geolocation)
Path Length (m)	obs_ort (geolocation)
GPS time (hrs)	obs_ort (geolocation)
Elevation (m)	igm_ort (geolocation)
Radiance $\mu W cm^{-2} Sr^{-1} nm^{-1}$	rdn_ort (geolocation)
Wavelength (nm)	rdn_ort.hdr (geolocation)
Full width half maximum (nm)	rdn_ort.hdr (geolocation)

Table 3: Symbols and Notation

Symbol	Value	Units
$L$	Spectral Radiance	$\mu W cm^{-2} Sr^{-1} nm^{-1}$
$E, F_o$	Spectral Irradiance	$\mu W cm^{-2} nm^{-1}$

$\rho$	Spectral Reflectance	Unitless; valid range 0-1
u	Water vapor column	$\text{g cm}^{-2}$
nmi	Nautical miles	A minute of latitude arc on the planet Earth is 1 nautical mile

### 3.3 Product Instances, Temporal/Spatial Resolution and Extent

A number of NEON data products derive directly from the atmospherically corrected reflectance. The atmospheric correction algorithm produces the product NEON.DOM.SIT.DP1G.30002.001.001.001. The instances, temporal/spatial resolution, and extent of each instance are listed in Table 4. Spatial resolution and extent are based on a flight altitude of 1000 m. AGL (above ground level).

Table 4: Instance, Temporal/Spatial Resolution and Extent

Instance	Temporal Resolution	Spatial Resolution	Extent
Reflectance	Annually	1 meter	5-20 km x 0.600 km x number of flightlines
Aerosol optical depth (@550 nm)	Annually	1 meter	5-20 km x 0.600 km x number of flightlines
Water Vapor Column	Annually	1 meter	5-20 km x 0.600 km x number of flightlines
Dark Dense Vegetation	Annually	1 meter	5-20 km x 0.600 km x number of flightlines
Visibility Index	Annually	1 meter	5-20 km x 0.600 km x number of flightlines
Illumination Factor	Annually	1 meter	5-20 km x 0.600 km x number of flightlines
Aspect	Annually	1 meter	5-20 km x 0.600 km x number of flightlines
Slope	Annually	1 meter	5-20 km x 0.600 km x number of flightlines
To-Sensor Zenith	Annually	1 meter	5-20 km x 0.600 km x number of flightlines
To-Sensor Azimuth	Annually	1 meter	5-20 km x 0.600 km x number of flightlines
Path Length	Annually	1 meter	5-20 km x 0.600 km x number of flightlines
Average Sun Zenith	Annually	1 meter	5-20 km x 0.600 km x number of flightlines
Average Sun Azimuth	Annually	1 meter	5-20 km x 0.600 km x number of flightlines
Sky View Factor	Annually	1 meter	5-20 km x 0.600 km x number of flightlines
Cast Shadow	Annually	1 meter	5-20 km x 0.600 km x number of flightlines
Haze-Cloud-Water Map	Annually	1 meter	5-20 km x 0.600 km x number of flightlines
Surface Elevation	Annually	1 meter	5-20 km x 0.600 km x number of flightlines
Flight Altitude	200 Hz	~0.25 m	5-20 km length x number of flightlines
Flight Heading	200 Hz	~0.25 m	5-20 km length x number of flightlines
Flight Time	200 Hz	~0.25 m	5-20 km length x number of flightlines

Title: NEON Imaging Spectrometer Radiance to Reflectance Algorithm Theoretical Basis Document		Date: 02/11/2015
NEON Doc. #: NEON.DOC.001288	Author: B. Karpowicz, T. Kampe	Revision: A

**3.3.1 Temporal Resolution and Extent**

The atmospheric correction algorithm is applied to each AOP flight line, which typically measure between 5 and 20km in length, and approximately 600m in width. Nominal flight speeds are 100 nmi/hr (185 km/hr), therefore the time required to acquire each flight line will range from 1.6 to 6.5 minutes. The NEON imaging spectrometer acquires a frame of data (~600 cross-track samples x ~ 420 spectral bands) 100 times every second (100Hz, or once every 100ms). On an operational basis, atmospherically corrected reflectance will be provided on a yearly basis for each AOP coverage area within a NEON domain that is surveyed annually.

**3.3.2 Spatial Resolution and Extent**

The atmospheric correction algorithm is applied to each AOP flight line, which typically measure between 5 and 20km in length, and approximately 600m in width. The Instantaneous Field of View (IFOV) of the NEON imaging spectrometer is 1.0 milliradian (mrad), which equates to a ground sampling distance (ignoring terrain effects) of 1m in the cross-track direction at a nominal flight altitude of 1000 m AGL. The actual ground sampling distance in the cross-track direction will vary with flight altitude angle from nadir, surface slope, and surface elevation. The along-track ground sampling distance is a bit more complicated to specify. While the imaging spectrometer’s spatial resolution in the along-track direction is still nominally 1m, the actual along-track ground sampling distance is a function of flight speed and detector integration rate. The NEON imaging spectrometer acquires data 100 times per second, while traveling nominally at 185 km/hr. As a result, the image will be over-sampled in the along-track direction with a ground sampling distance of 0.5m and with a ground footprint of 1m resolution at the nominal flight altitude. However, the actual ground sampling distance will be dependent upon flight altitude, speed of the aircraft, and surface elevation. Since the radiance has been orthorectified and resampled to a 1 meter grid, the reflectance product will be provided at a 1 meter resolution. The current method used in the orthorectification process takes the last pixel recorded in the along-track dimension, and disregards previously oversampled pixels. For example, if three along-track spectrometer pixels fall within the same one meter grid, only the last pixel recorded will be retained. In the future, this approach may change to utilize more of the recorded spectrometer radiance.

An additional complication that comes into play with respect to spatial resolution is the adjacency effect (*Richter et al., 2006*). Even after the effects of the atmosphere within each spectrometer IFOV are removed, radiance scattered by the air volume over neighboring pixels

Title: NEON Imaging Spectrometer Radiance to Reflectance Algorithm Theoretical Basis Document		Date: 02/11/2015
NEON Doc. #: NEON.DOC.001288	Author: B. Karpowicz, T. Kampe	Revision: A

can contribute to the radiance measured in a spectrometer IFOV. Some atmospheric correction algorithms attempt to remove the effect (including the algorithm specified in this document), however, without perfect knowledge of atmospheric composition and temperature, information from neighboring pixels may remain as a residual error. Therefore, the spatial footprint contributing to the radiance measured by a single imaging spectrometer pixel will extend outside the nominal 1m resolution (i.e., spectra from a neighboring pixel be convolved with the desired spectra of a given pixel).

## 4 SCIENTIFIC CONTENT

### 4.1 Theory of Measurement/Observation

The fundamental measurement made by the NEON imaging spectrometer is that of spectral radiance (as described in the NEON Imaging Spectrometer (NIS) Level 1B Calibrated Radiance ATBD, RD [03]). The property of interest which relates to surface properties (vegetation, soil, mineralogy, etc.) is surface spectral reflectance ( $\rho$ ). The apparent reflectance is defined as

$$\rho = \frac{\pi L}{\cos(\theta_0)F_0} \quad (1)$$

where  $L$  is the spectral radiance ( $\mu Wcm^{-2}sr^{-1}nm^{-1}$ ) reflected back towards the sensor,  $\theta_0$  is the solar zenith angle, and  $F_0$  is the extraterrestrial solar spectral irradiance ( $\mu Wcm^{-2}nm^{-1}$ ). In the absence of an atmosphere, the reflectance properties could be derived directly (the radiance measured at the sensor would be directly reflected back to the sensor). However, as shown in Figure 4, the atmosphere adds a great deal of complexity to the relationship between radiance measured by the sensor and the surface reflectance properties. In this figure, the blue line represents light scattered into the sensor's instantaneous field of view (IFOV) without having been reflected off the surface target (also referred to as path radiance  $L_p$ ). The dark green line represents light (direct + diffuse) reflected to the sensor from the surface targets within the IFOV. Finally, the light green line represents light reflected in the neighborhood of the desired IFOV (the adjacency effect). The goal of the atmospheric correction algorithm is to extract the radiance signature of the atmosphere, leaving spectral information from the reflectance versus wavelength from surface targets such as vegetation, soil, and mineral properties. To achieve this goal, the influence from the atmosphere in the retrieved surface reflectance must be removed.

Title: NEON Imaging Spectrometer Radiance to Reflectance Algorithm Theoretical Basis Document		Date: 02/11/2015
NEON Doc. #: NEON.DOC.001288	Author: B. Karpowicz, T. Kampe	Revision: A

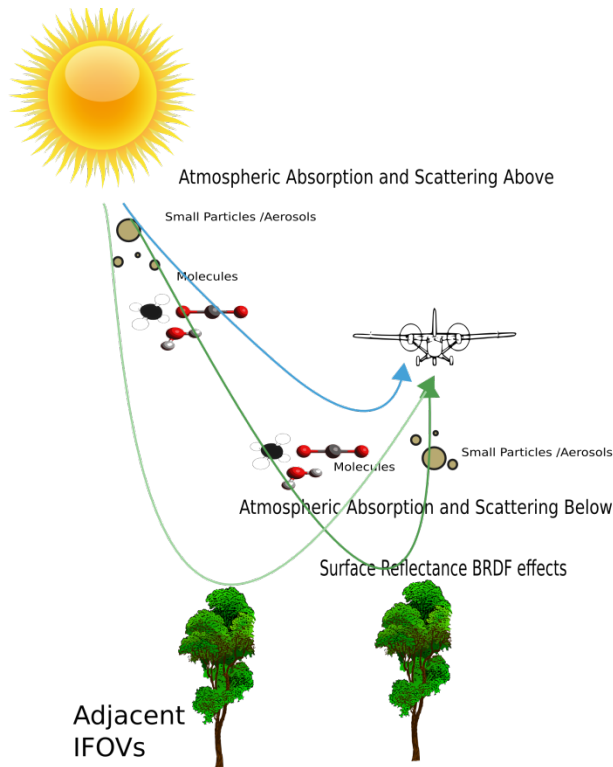


Figure 4: Illustration of the atmospheric correction process.

## 4.2 Theory of the Algorithm

Fundamentally, the theory of atmospheric correction relies upon a radiative transfer model to derive the atmospheric transmittance. The radiative transfer model must include molecular absorption and scattering, along with aerosol absorption and scattering. The current atmospheric correction algorithm, ATCOR, uses a lookup table derived from the MODTRAN 5 radiative transfer code (ER [02]). This database is used to correct for first-order atmospheric effects. The algorithm also has a few additional functions that compensate for effects such as Bidirectional Reflectance Distribution Function (BRDF), aerosol variability, water vapor variability, and adjacency effects. All of these are described in detail within this document.

## 5 ALGORITHM IMPLEMENTATION

A summary of the typical ATCOR process flow is shown in Figure 5. The first step in the process is to read in all the required lookup tables and radiance data. The details of how the lookup tables are generated are summarized in Sections 5.1 and 5.2. The next step in the process flow is to mask and remove haze (regions of high optical depth) as described in Section 5.6. This is an

<i>Title:</i> NEON Imaging Spectrometer Radiance to Reflectance Algorithm Theoretical Basis Document		<i>Date:</i> 02/11/2015
<i>NEON Doc. #:</i> NEON.DOC.001288	<i>Author:</i> B. Karpowicz, T. Kampe	<i>Revision:</i> A

optional step typically performed by an analyst, and is not part of the typical batch runs using ATCOR. The next step is to remove cloud shadow as described in Section 5.7. This step is optional, as the algorithm in ATCOR can result in some undesirable effects in dark terrain. Following this, a water body mask (lakes, rivers, streams, etc.) is generated using a threshold criteria described in Section 5.3. Following the development of a water body mask, aerosol retrieval is performed using dark dense vegetation (excluding the water body mask in the previous step) as described in Section 5.3. Once the aerosol retrieval is performed, an analyst may decide to change the aerosol model based on the aerosol type retrieval as described in Section 5.3. Next, water vapor retrieval is performed using the method described in Section 5.4. Once the water vapor retrieval is performed, the atmospheric constituent lookup tables are updated using an optimal value for total column water vapor. Once a water vapor map has been calculated, the next step is to iteratively perform the reflectance retrieval described in Sections 5.8 and 5.9. This reflectance retrieval accounts for both adjacency and terrain effects. A final optional step available is to use the Bidirectional Reflectance Function (BRDF) correction built into ATCOR as described in Section 5.5. Currently, this is not used in the standard NEON data stream as further work needs to be done to evaluate what BRDF scheme is appropriate for NEON data.

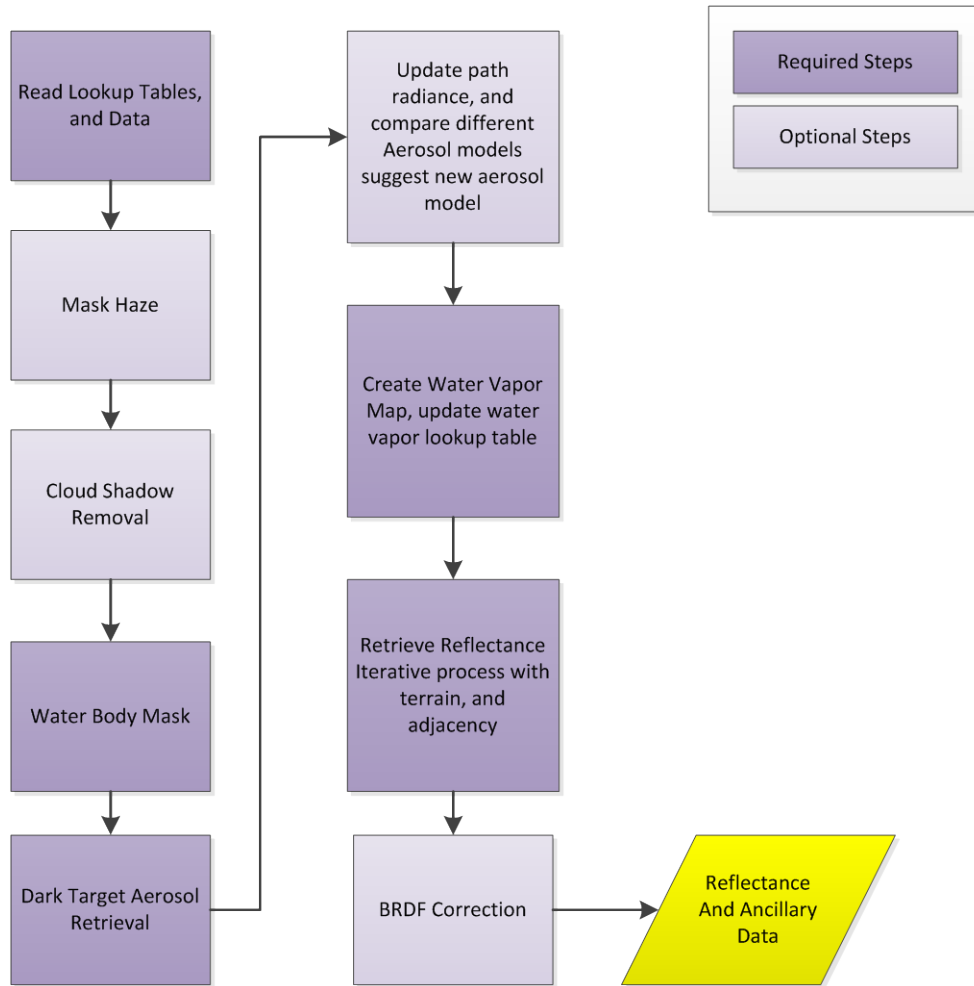


Figure 5: Atmospheric Correction Steps in ATCOR

## 5.1 Atmospheric Transmission Computation

The atmospheric transmittance database included in ATCOR is based upon MODTRAN5 (ER [02]). The database is a large 6.2 GB file which is resampled by the ATCOR RESLUT routine down to 10-50 MB depending upon the spectral resolution of the sensor. The wavelength spacing is variable depending upon the wavelength region. The sampling approach is summarized in Table 5. The sampling approach used by ATCOR was designed to be appropriate for sensors with a bandwidth >2 nm operating in the solar region from 340–2540 nm. This is appropriate for the NEON imaging spectrometer which has a spectral sampling of 5 nm. The MODTRAN runs were completed in units of wavenumber, which results in an irregular grid in wavelength space. To

Title: NEON Imaging Spectrometer Radiance to Reflectance Algorithm Theoretical Basis Document		Date: 02/11/2015
NEON Doc. #: NEON.DOC.001288	Author: B. Karpowicz, T. Kampe	Revision: A

re-grid the MODTRAN runs, the final lookup table used by the RESULT routine internal to ATCOR is resampled with 0.4 nm FWHM Gaussian functions at a sampling interval of 0.4 nm.

Table 5: ATCOR spectral sampling in monochromatic database.

Wavelength Region (nm)	Spectral Sampling (nm)
340-1349	0.40
1351-1449	0.98
1780-1949	1.74
1949-2540	0.40

The lookup table contains 8 Flight altitudes (0.1, 1, 2, 3, 4, 5, 10, and 20 km). If a flight altitude is between these flight altitudes, ATCOR will interpolate the lookup table (i.e., if a flight altitude of 1.5 km is entered ATCOR will interpolate between 1 km and 2 km to derive the appropriate lookup table). An additional lookup table exists for a 99 km altitude for satellite sensors. The water vapor database contains 5 values (0.4, 1.0, 2.0, 2.9, 4.0 g/cm<sup>2</sup>). This range of values is used by the water vapor retrieval algorithm along with spectral information to either interpolate or extrapolate the water vapor amount on a per-pixel basis. The CO<sub>2</sub> mixing ratio is set at 400 ppmv, and the O<sub>3</sub> amount is set to 330 Dobson Units.

## 5.2 Extraterrestrial Solar Irradiance Curve Source

The extraterrestrial solar irradiance recommended by the authors of ATCOR is that of *Fontenla et al.* (2011). The original source spectrum from *Fontenla et al.* (2011) (resolution 0.1 cm<sup>-1</sup>) is convolved in ATCOR with Gaussian response functions with FWHM values of 0.4 nm, and a grid spacing of 0.4 nm. Alternatively, the user can use a solar spectrum derived from *Kurucz* (2005), or any other desired source. For sources other than *Fontenla et al.* (2011), or *Kurucz* (2005) the user will need to convert the spectral database using a utility in the “tools” panel.

The *Fontenla et al.* (2011) extraterrestrial solar irradiance is used in the standard NEON imaging spectrometer processing chain.

## 5.3 Aerosol Retrieval

Given that the path radiance will vary depending upon aerosol type, viewing geometry, and solar illumination, these must be taken into account for accurate determination of radiance. The approach used in ATCOR is to use a second-order polynomial to fit the scattering angle dependence for each type of aerosol.

Title: NEON Imaging Spectrometer Radiance to Reflectance Algorithm Theoretical Basis Document		Date: 02/11/2015
NEON Doc. #: NEON.DOC.001288	Author: B. Karpowicz, T. Kampe	Revision: A

For sensors like the NIS that have bands in the 1.6 μm and 2.2 μm regions, a variation of the MODIS dark target algorithm (*Kaufman et al., 1997*) is used to retrieve aerosol properties. The MODIS dark-target algorithm was developed to infer clear-sky (i.e., non-cloudy) aerosol properties over land surfaces that have low surface reflectance values. The 2.2 μm band was selected since it is unaffected by emission of infrared radiation and the accurate detection of dark pixels is not inhibited by the effect of aerosols.

Since most aerosol types (except mineral dust) are smaller than 1.0 μm in diameter, the 2.2 μm wavelength is much larger than the aerosol particles and therefore the aerosols will be transparent to solar radiation at 2.2 μm. This can be best understood by considering the scattering efficiency,  $Q_s$ , as defined by the Lorenz-Mie theory of scattering by spheres (*van de Hulst, 1957*), where  $Q_s$  is defined as

$$Q_s = \frac{\sigma_s}{\pi a^2} = c_1 x^4 (1 + c_2 x^2 + c_3 x^3 + \dots) (1 + c_2 x^2 + c_3 x^3 + \dots) \quad (2)$$

Where:  $\sigma_s$  is the particle scattering cross section,  
 $a$  is the particle radius,  
 $x$  is the particle size parameter and is defined as  $x = 2\pi a/\lambda$ ,  
 $\lambda$  is the wavelength of light, and for the case of nonabsorbing particles the coefficients are given by

$$c_1 = \frac{8}{3} \left( \frac{m^2 - 1}{m^2 + 2} \right),$$

$$c_2 = \frac{6}{5} \left( \frac{m^2 - 1}{m^2 + 2} \right),$$

$$c_3 = \frac{3}{175} \left[ \frac{m^6 + 41m^4 - 28m^2 + 284}{(m^2 + 2)^2} \right] + \frac{1}{900} \left[ \frac{m^2 + 2}{2m^2 + 2} \right]^2 [15 + (2m^2 + 3)^2],$$

where  $m$  is the refractive index of the particle.

In the case of Rayleigh, or molecular scattering, particle radii  $a$  are approximately  $10^{-4}$  μm, therefore  $x \approx 10^{-3}$  at visible wavelengths. Thus, the higher order terms in equation (2) can be neglected and the scattering efficiency is proportional to  $\lambda^{-4}$ . Also, molecular scattering is negligible at a wavelength of 2.2 μm. because  $x \ll 1$ . Similarly for aerosols,  $a \approx 10^{-1}$  μm,  $x \approx 1$  in the visible, and  $x \approx 0.25$  at a wavelength of 2.2 μm. Therefore, the scattering efficiency for

Title: NEON Imaging Spectrometer Radiance to Reflectance Algorithm Theoretical Basis Document		Date: 02/11/2015
NEON Doc. #: NEON.DOC.001288	Author: B. Karpowicz, T. Kampe	Revision: A

aerosol particles is also low ( $Q_s \approx 0.004$  at  $2.2\mu\text{m}$ ) and aerosols are transparent at this wavelength.

The key assumption with the dark target algorithm is that the surface reflectance in the near infrared band is close to the apparent reflectance at the sensor. The algorithm starts by removing pixels with strong water vapor absorption. The first set of criteria for selecting dark pixels requires that the SWIR reflectance values are greater than 1% (the minimum reflectance criteria at 1.6, or  $2.2\mu\text{m}$ ), and the Normalized Difference Vegetation Index (NDVI) must be greater than 0.1 (where  $\text{NDVI} = (\rho_{850^-} - \rho_{650}) / (\rho_{850^+} + \rho_{650})$ ). This ensures that only dark soils and vegetation are included in the aerosol retrieval, while the reflectance from water bodies is excluded. The upper SWIR reflectance threshold is variable, and depends upon the percent of pixels included from the entire image. If the  $2.2\mu\text{m}$  SWIR band is available, the threshold is set to 5% reflectance. If the number of reference pixels is less than 1% of the image using a 5% reflectance threshold, the reflectance threshold is increased to 10%, or finally 12%, if the 1% of total image coverage criteria is not met at each step. If a  $2.2\mu\text{m}$  band is unavailable, the  $1.6\mu\text{m}$  SWIR band is used. The upper reflectance thresholds are adjusted until 1% of total image coverage criteria is reached (threshold values include 10, 15, and 18%). A regression analysis by *Kaufman et al.* (1997) showed that dark vegetated surfaces follow a decreasing reflectance with decreasing wavelength comparing blue and red channels to a  $2.2\mu\text{m}$  band. A similar approach was taken by *Richter and Schläpfer* (2011) using blue and red bands in conjunction with a  $1.6\mu\text{m}$  band. The regression analysis gave the following relations for the  $2.2\mu\text{m}$  band regression

$$\rho_{red} = 0.5\rho_{2.2\mu\text{m}} \quad (3)$$

$$\rho_{blue} = 0.5\rho_{red} \quad (4)$$

The  $1.6\mu\text{m}$  band regression showed the following relations for the red and blue bands

$$\rho_{red} = 0.25\rho_{1.6\mu\text{m}} \quad (5)$$

$$\rho_{blue} = 0.5\rho_{red} \quad (6).$$

Generally, the  $2.2\mu\text{m}$  regression is used if radiance in this band is retrieved. This is the case for the NIS imaging spectrometer (spectral range is 380 to 2510 nm) so the  $2.2\mu\text{m}$  regression is used for standard processing.

Title: NEON Imaging Spectrometer Radiance to Reflectance Algorithm Theoretical Basis Document		Date: 02/11/2015
NEON Doc. #: NEON.DOC.001288	Author: B. Karpowicz, T. Kampe	Revision: A

Using the surface reflectance values derived from the SWIR, the algorithm uses a lookup table of radiance to compute the visibility (optical depth) in the red, and blue bands. The path radiance is then adjusted using

$$L_{p,blue}^{update} = L_{p,blue} - \frac{\tau_{blue}\rho_{blue}E_{g,blue}}{\pi} \quad (7)$$

$$L_{p,red}^{update} = L_{p,red} - \frac{\tau_{red}\rho_{red}E_{g,red}}{\pi} \quad (8)$$

where  $L_p$  is the path radiance,  $\tau$  is the optical depth and  $E_g$  is the global flux in units of  $\mu Wcm^{-2}nm^{-1}$ , the sum of the direct and diffuse solar irradiance contributions.

An option available in ATCOR in the interactive GUI mode is to determine the aerosol type. This depends upon the corrected red and blue path radiance in Equations 7 and 8, the values can be compared to the standard MODTRAN aerosol types to determine which aerosol type best matches the scene. This correction is done to isolate the aerosol contribution to the radiance signal (the path radiance is defined as the blue line in Figure 4; molecular scattering is included and is independent of aerosol contributions). The double ratio is calculated using

$$d_p = [L_{p,blue,scene}/L_{b,red,scene}]/[L_{p,blue,MODTRAN}/L_{p,red,MODTRAN}] \quad (9)$$

The MODTRAN aerosol type that is closest to a  $d_p$  value of 1.0 is chosen to be the best aerosol type. If the difference between  $L_{p,blue,scene}$  and  $L_{p,blue,MODTRAN}$  is greater than 5%, then  $L_{p,blue,scene}$  is used as the path radiance. The path radiance in bands between the blue to red regions is rescaled using

$$BR_{scale} = L_{p,blue,scene}/L_{p,blue,MODTRAN} \quad (10)$$

Typically, the aerosol type determination is only performed once for a site.

While it is possible to manually set aerosol properties (i.e., take a visibility measurement from a photometer and set it for an ATCOR correction), it has been found that errors arise that include values of negative reflectance can be produced by ATCOR if the dark target algorithm isn't selected. Therefore, this option is not being implemented in the standard processing of NEON data.

## 5.4 Water Vapor Retrieval

The water vapor column retrieval is either performed using the atmospheric precorrected differential absorption algorithm (APDA) (Schläpfer *et al.*, 1998), or a Linear Regression Ratio (LIRR) (Schläpfer *et al.*, 1996). Both techniques attempt to correlate the amount of total column

Title: NEON Imaging Spectrometer Radiance to Reflectance Algorithm Theoretical Basis Document		Date: 02/11/2015
NEON Doc. #: NEON.DOC.001288	Author: B. Karpowicz, T. Kampe	Revision: A

water vapor to the depth of the water vapor absorption feature observed in the spectrometer data. The ATCOR authors recommend the APDA method and this is the algorithm used for standard processing.

The APDA technique uses three bands: one in the water vapor absorption band (either 940 or 1130 nm), and the others in neighboring window regions. It should be noted that all aerosol corrections must be done prior to water vapor correction, since the neighboring bands are dependent upon aerosol optical depth. The APDA ratio is defined as

$$R_{APDA}(\rho, u) = \frac{L_2(\rho_2, u) - L_{2,\rho}(u)}{w_1(L_1(\rho_1) - L_{1,\rho}) + w_3(L_3(\rho_3) - L_{3,\rho})} \quad (11)$$

where  $L$ ,  $L_p$  and  $u$  represent the total at-sensor radiance, path radiance, and water vapor column, respectively. Subscript 2 represents the band with strong water vapor absorption (e.g., 910-950 nm), while subscripts 1, and 3 represent window regions (e.g., 850-890 nm, 1010-1050 nm). The weighting factors ( $w_1$  and  $w_2$ ) are computed using

$$w_1 = \frac{\lambda_3 - \lambda_2}{\lambda_3 - \lambda_1} \quad \text{and} \quad w_3 = \frac{\lambda_2 - \lambda_1}{\lambda_3 - \lambda_1} \quad (12)$$

where the surface reflectance in the water vapor absorption band ( $\rho_2$ ) is unknown. The neighboring bands 1 and 3 are used to linearly interpolate the value of  $\rho_2$ . The linear interpolation is written as

$$\rho_2 = w_1\rho_1 + w_3\rho_3 \quad (13)$$

The  $R_{APDA}$  ratio is given by

$$R_{APDA} = \frac{\rho_2 \tau_2 E_{g_2}(u)}{\rho_2 \tau_2(u=0) E_{g_2}(u=0)} = \frac{\tau_2(u) E_{g_2}(u)}{\tau_2(u=0) E_{g_2}(u=0)} \quad (14)$$

The APDA ratio,  $R_{APDA}$ , is then expressed in terms of an exponential function for varying amounts of total column water vapor

$$R(u) = \exp(-\alpha + \beta \sqrt{u}) \quad (15)$$

which is solved for  $u$  to give the resulting estimate of water vapor column:

Title: NEON Imaging Spectrometer Radiance to Reflectance Algorithm Theoretical Basis Document		Date: 02/11/2015
NEON Doc. #: NEON.DOC.001288	Author: B. Karpowicz, T. Kampe	Revision: A

$$u = \left( \frac{\alpha + \ln(R)}{\beta} \right)^2 \quad (16)$$

where  $\alpha$  and  $\beta$  are determined from 5 vapor column amounts computed in ATCOR.

The stated accuracy of the water vapor retrieval is about 5–10% for the APDA method (*Richter and Schlapfer, 2008*). Values of water vapor column are computed for each pixel, and are used as an input to the atmospheric transmission lookup table. The spectral absorption due to the water vapor column is then accounted for in the spectral reflectance retrieval.

## 5.5 BRDF Correction

The correction for the Bidirectional Reflectance Distribution Function (BRDF<sup>2</sup>) is not currently implemented as part of the standard atmospheric correction processing for the NEON imaging spectrometer. The description of this processing is presented herein for informational purposes only.

There are two methods available for BRDF correction in ATCOR. The first is the Nadir Normalization method that is applicable to flat surfaces. The second is the empirical BRDF correction in rugged terrain.

### 5.5.1 Nadir Normalization Method

The nadir normalization method begins with the definition of nadir as pixels within +/-3° of nadir. For a given pixel, the brightness (or radiance) is resampled in 3° intervals, except in cases where there is a hot spot (bright region resulting when sun and view directions coincide) in which case the brightness is resampled in 1° increments. The nadir normalized brightness value for scan line is calculated as

$$b_{norm} = b(j) \frac{b_{average,nadir}}{f_2(j)} \quad (17)$$

Where  $b(j)$  are the radiance values at the specified angular increments,  $b_{average,nadir}$  is the average brightness for the nadir region, and  $f_2(j)$  is a function computed using the following steps:

---

<sup>2</sup> BRDF Explained: [http://www.umb.edu/spectralmass/terra\\_aqua\\_modis/modis](http://www.umb.edu/spectralmass/terra_aqua_modis/modis)

Title: NEON Imaging Spectrometer Radiance to Reflectance Algorithm Theoretical Basis Document		Date: 02/11/2015
NEON Doc. #: NEON.DOC.001288	Author: B. Karpowicz, T. Kampe	Revision: A

1. The  $b(j)$  values are averaged over  $3^\circ$  (no hot spot) or  $1^\circ$  (with hot spot) intervals resulting in a function with  $m+1$  grid points for the  $m$  off nadir intervals plus the nadir interval.
2. An interpolation from the  $3^\circ$  grid to the  $1^\circ$  grid is performed (if no hot-spot is in near the geometry).
3. A moving averaging window is applied over a  $5^\circ$  window (without hot spot present), or a  $3^\circ$  interval (with hot spot present).

Application of this algorithm therefore provides a normalization of the scan angle-dependent brightness values to the nadir value.

### 5.5.2 Empirical BRDF in Rugged Terrain

The Nadir Normalization method described in the previous section is limited to situations over flat terrain. However, mountainous regions exhibit large variations in terrain slope causing variations in bidirectional brightness in vegetated regions. In this case, the simple Lambertian assumption of the reflectance is inadequate and leads to overcorrected reflectance in faintly illuminated areas (ER [03]). The ATCOR-4 program incorporates an empirical BRDF correction algorithm that is applicable to scenes containing rugged terrain.

The empirical geometric BRDF correction factor is defined as

$$G = \left( \frac{\cos \beta_i}{\cos \beta_T} \right)^b \geq g \quad (18)$$

where  $\beta_i$  is the solar incidence angle,  $\beta_T$  is the threshold illumination angle, and  $g$  is the lower bound for  $G$ . The variables  $\beta_T$ ,  $b$  and  $g$  are specified by the user. The threshold illumination angle is used to control how rapidly the response function  $G$  will vary as a function of illumination angle. It should have some margin relative to the solar zenith angle and is nominally set at 20 degrees greater than the solar zenith angle  $\Theta_s$  when  $\Theta_s$  is less than  $45^\circ$ . The exponent value  $b$  can be varied by in discrete values of  $1/3$ ,  $1/2$ ,  $3/4$  or 1.

In most cases, a value of  $g$  between 0.2 and 0.25 is appropriate. In extreme cases, it may be necessary to set  $g$  to 0.1. Values of  $G > 1$  are set to 1.0, and values of  $G$  less than  $g$  are set to  $g$ . Once  $G$  is found it is applied to the reflectance value found assuming a Lambertian surface ( $\rho_L$ , the reflectance value found through the standard ATCOR process) to yield the corrected reflectance,  $\rho_g$ :

$$\rho_g = G\rho_L \quad (19)$$

Title: NEON Imaging Spectrometer Radiance to Reflectance Algorithm Theoretical Basis Document		Date: 02/11/2015
NEON Doc. #: NEON.DOC.001288	Author: B. Karpowicz, T. Kampe	Revision: A

## 5.6 Haze Removal

Generally speaking, the aerosol contribution in the lookup tables for ATCOR is generated with relatively low values for optical depth. Often times there are regions within an image that have significantly higher values for optical depth, resulting in regionally hazy images. In the nominal processing sequence, haze removal is not implemented. Images identified with excessive haze will need to be identified as part of the quality control process and processed off-line.

The regional haze is something which must be identified by the analyst. For example, there may be a region of white haze that remains after applying the nominal atmospheric correction algorithm. In this case, the haze removal algorithm can be applied to improve the quality of the atmospheric correction if deemed necessary. The algorithm implemented in ATCOR is known as the “Tassled Cap Transformation” (TCT.) and can be run automatically within ATCOR. The algorithm is described in more detail in *Crist and Cicone (1984)*, *Richter (1996)*, and *Zhang et al. (2002)*.

Clear and Hazy areas are masked using

$$TC = x_1 * BLUE + x_2 * RED \quad (20)$$

Where  $TC$  is the Tassled Hat coefficient,  $BLUE$  is the Blue band,  $RED$  is the red band, and  $x_1$  and  $x_2$  are the associated weighting coefficients. The  $RED$ , and  $BLUE$  radiance bands are chosen by ATCOR as the bands with center wavelengths closest to Red (~650 nm), and Blue (~475 nm). This is a slight departure from the original TCT algorithm in that in this case, narrow hyperspectral radiance bands are used in place of wider spectral bands typical of multispectral sensors (e.g., Landsat, MODIS). Clear area pixels are defined as those pixels where  $TC$  is less than the mean value of  $TC$ .

Once clear and hazy areas are defined, the red and blue radiance bands are regressed against one another (red y-axis, blue x-axis). The slope of the line  $\alpha$  is found via the regression between the red and blue channel.

It is assumed that haze areas are orthogonal to the “clear line” defined by the red-blue regression. The haze optimized transform,  $HOT$ , is defined (*Zhang et al., 2002*) as

$$HOT = BLUE * \sin\alpha - RED * \cos\alpha \quad (21)$$

Values for  $HOT$  are then computed for the image. For each band below 800 nm, a histogram of  $HOT$  is generated with narrow bins of radiance values ( $j$  levels). The haze signal  $\Delta$  to be

Title: NEON Imaging Spectrometer Radiance to Reflectance Algorithm Theoretical Basis Document		Date: 02/11/2015
NEON Doc. #: NEON.DOC.001288	Author: B. Karpowicz, T. Kampe	Revision: A

subtracted from the radiance  $L$  corresponding to  $HOT(\text{level } j)$  minus the radiance corresponding the lower 2% of the  $HOT$  (i.e., haze areas). The de-hazed digital number is then given by

$$L_{dehazed} = L - \Delta \quad (22)$$

The mask for the application of  $L_{dehazed}$  is defined by one of two methods. A large area haze mask (defined by a lower threshold for  $HOT$ , and recommended for most cases) is defined by

$$HOT > \text{mean}(HOT) - 0.5 * \text{std}(HOT) \quad (23)$$

Alternatively, a smaller area haze mask, defined as

$$HOT > \text{mean}(HOT). \quad (24)$$

can also be used, when the haze is confined to a more limited area. Currently, a small area is defined as less than 1 square kilometer in extent, and a large area as greater than 1 km<sup>2</sup>. Which mask to use is not stringently defined although the large area haze mask is stated to be superior for most cases (ER [03]). An example of the benefit of haze correction is shown in Figure 10.18 in ER [03]. Additional examples can be viewed on the ATCOR web site (<http://www.rese.ch>).

Ideally, one would use the same haze removal algorithm over land and water, but this is generally not feasible. Since the NEON mission is to survey terrestrial ecosystems, it is not anticipated that the retrieval of spectroscopic data over extended water bodies will be a normal part of the mission. However, the NEON overflights will occur over small water bodies (e.g., lakes, streams) during surveys and it may become important to remove haze or sun glint over this water bodies in such cases. Haze removal over water is not implemented as part of the nominal NEON atmospheric correction processing flow, but is available in ATCOR as an option to be applied off line in rare or unusual circumstances. This would occur after quality assessment of an individual flight line. The haze removal algorithm in ATCOR uses a near infrared band to estimate the spatial distribution of haze over water. This algorithm is described in Yi (2008).

## 5.7 Cloud Shadow Removal

By default, shadow correction is not implemented in the standard NEON data processing stream. During AOP operations, every effort will be made to collect data which is cloud free. However, there may be situations where the appearance of pixels with clouds, or cloud shadows is unavoidable. In these cases, the analyst may decide to use the cloud shadow removal algorithm.

Title: NEON Imaging Spectrometer Radiance to Reflectance Algorithm Theoretical Basis Document		Date: 02/11/2015
NEON Doc. #: NEON.DOC.001288	Author: B. Karpowicz, T. Kampe	Revision: A

An option available in ATCOR allows for de-shadowing of pixels using a matched filter algorithm described in *Richter and Müller (2005)*. The matched filter algorithm uses the correlation between a known signal, or template, with an unknown signal to detect the presence of the template in the unknown signal<sup>3</sup>. Ultimately, the goal of the algorithm is to modify the direct solar radiance term ( $E_{dir}$ ) to correct for shadows. The ideal solution would be to apply a filter that would change the direct illumination term to zero, and thus the reflectance could be calculated with the diffuse term only. The approach taken by ATCOR is to develop a matched filter that aims to identify regions where the reflectance is zero.

The process is shown in Figure 6. As a first step the reflectances at 0.48, 0.85, 1.6, and 2.2  $\mu\text{m}$  are computed using

$$\rho = \frac{\pi d^2 L_{sensor} - L_{path}}{T(E_{dir} + E_{dif})} \quad (25)$$

where  $d$  is the sun-earth distance (1 astronomical unit),  $L_{sensor}$  is the at-sensor radiance,  $L_{path}$  is the path radiance (scattered component of radiance reaching the sensor, without having contact with the ground),  $T$  is the ground to sensor transmittance, and  $E_{dir}$  and  $E_{dif}$  are the direct and diffuse radiance components.

The next step is to identify those pixels that contain clouds or water bodies so that they are not misidentified as shadow. This is done by setting threshold values for the reflectance. If the reflectance is less than 5% at 0.85  $\mu\text{m}$  or less than 1% at 1.6  $\mu\text{m}$ , the pixel is classified as a water pixel and is removed from the shadow correction algorithm. If the reflectance is greater than 30% at 0.48  $\mu\text{m}$  or 1.6  $\mu\text{m}$ , the pixel is classified as cloudy and is removed from consideration in the shadow correction algorithm. This allows for the determination of the reflectance at 0.85, 1.6, and 2.2  $\mu\text{m}$  that is composed of cloud-free and water-body free pixels.

Once the water-filled and cloudy pixels have been removed from consideration, the covariance matrix of  $\rho$  ( $C(\rho)$ , abbreviated here as  $C$ ) is used to compute a matched filter tuned to a specific target reflectance  $\rho_t$  as done in *Adler-Golden et al.(2002)*:

---

<sup>3</sup> Matched filter: see [http://en.wikipedia.org/wiki/Matched\\_filter](http://en.wikipedia.org/wiki/Matched_filter)

Title: NEON Imaging Spectrometer Radiance to Reflectance Algorithm Theoretical Basis Document		Date: 02/11/2015
NEON Doc. #: NEON.DOC.001288	Author: B. Karpowicz, T. Kampe	Revision: A

$$V_{matchedfilter} = \frac{C^{-1}(\rho_t - \bar{\rho})}{(\rho_t - \bar{\rho})^T C^{-1}(\rho_t - \bar{\rho})} \quad (26)$$

where  $\bar{\rho}$  is the average reflectance for the scene neglecting water/cloud pixels, and  $\rho_t$  is the target reflectance. A simplified form of the matched filter with where the target reflectance  $\rho_t$  is set to zero is given by

$$V_{shadow} = \frac{C^{-1}\bar{\rho}}{(\bar{\rho})^T C^{-1}\bar{\rho}} \quad (27)$$

where  $V_{shadow}$  is a function which will be zero for regions where a shadow exists, and 1.0 where no shadow is present. Unfortunately, as partially shadowed pixels enter into the mean reflectance, this results in negative values for  $V_{shadow}$ .

Using Equation 35, the unscaled shadow function  $\Phi(x,y)$  is defined as

$$\Phi(x,y) = V_{shadow} (\rho(x,y) - \bar{\rho}) \quad (28)$$

Ideally, this function would be 0 for regions which are not directly illuminated and 1 for regions of direct illumination. The negative values resulting from the matched-filter approach need to be re-scaled to physical values. The histogram of  $\Phi(x,y)$  is used to rescale  $\Phi(x,y)$  to  $\Phi^*(x,y)$ . This step is necessary to derive a scale factor for all pixels which are not identified as either containing a cloud, or water body. This scale factor can then be applied to modify the direct surface radiance  $E_{dir}$ .

$$\Phi^*(x,y) = \frac{\Phi - \Phi_{min}}{\Phi_{max} - \Phi_{min}} \quad \text{when } \Phi \leq \Phi_{max} \quad (29)$$

$$\Phi(x,y) = 1 \quad \text{when } \Phi > \Phi_{max} \quad (30)$$

The process to determine the values of  $\Phi_{max}$  and  $\Phi_{min}$  is shown in Figure 6. Nominally, the smaller peak associated with shadow filled pixels ( $\Phi_2$ ) is used to determine the threshold ( $\Phi_T$ ). The threshold determines whether or not a pixel is considered to be in the core shadow area. The nominal core shadow area is then expanded by an additional 100 meters by default to avoid edge effects. The corrected shadow function,  $\Phi^*(x,y)$ , is then applied to pixels that are below the  $\Phi_T$  threshold value using

Title: NEON Imaging Spectrometer Radiance to Reflectance Algorithm Theoretical Basis Document		Date: 02/11/2015
NEON Doc. #: NEON.DOC.001288	Author: B. Karpowicz, T. Kampe	Revision: A

$$\rho = \frac{\pi d^2 L_{sensor}(x, y) - L_{path}}{T(\Phi^*(x, y)E_{dir} + E_{dif})} \quad (31)$$

to remove the shadow from the shadowed pixels. Since the de-shadowing match filter is not a perfect shadow transformation, it is recommended that the de-shadowing algorithm be restricted to the most-likely shadowed areas to minimize the number of misclassifications.

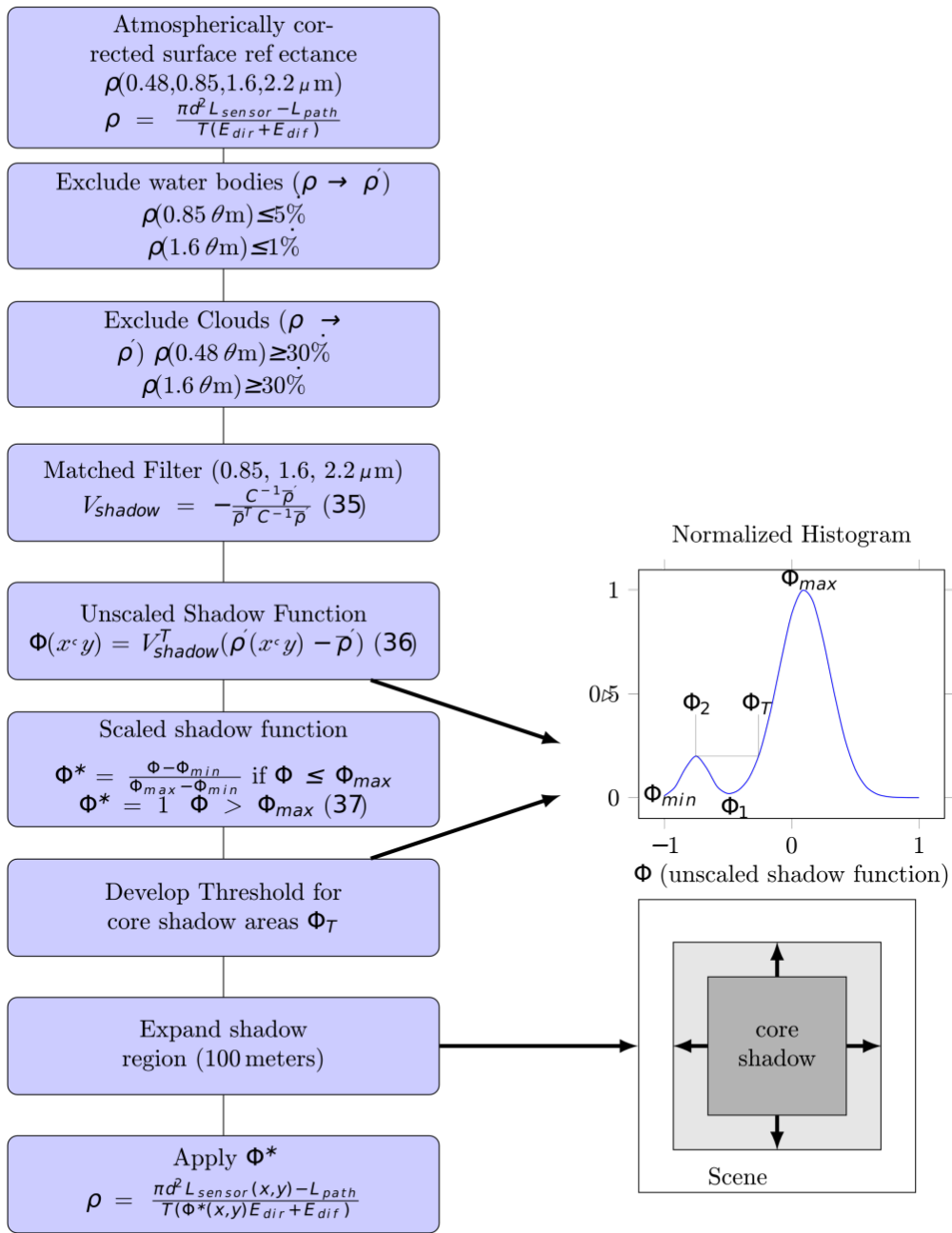


Figure 6: Flowchart describing the cloud shadow removal process.

## 5.8 Adjacency Effect Correction

### 5.8.1 Atmospheric Correction with Adjacency Effect assuming Flat Terrain

The adjacency effect is the physical phenomenon that results in spectral contamination within a pixel due to radiation reflected from neighboring pixels being scattered into the instantaneous field of view of a pixel. As shown in Figure 7, there are a number of contributors to the radiation field seen by an individual pixel. Radiation component 1 represents the path radiance (i.e., photons that don't reach the ground but are scattered in the air volume between the sensor and the ground). Component 2 is the total (direct plus diffuse) solar radiation reflected from the target and transmitted to the sensor. Components 3 and 4 represent the contributors due to the adjacency effect – (3) the reflected background radiation scattered into the detector instantaneous field of view and (4) the radiation backscattered to the ground by the atmosphere and eventually into the detector instantaneous field of view. Only the second term contains information on the target surface reflectance to be retrieved. The other contributors need to be calculated and removed as part of the atmospheric correction retrieval.

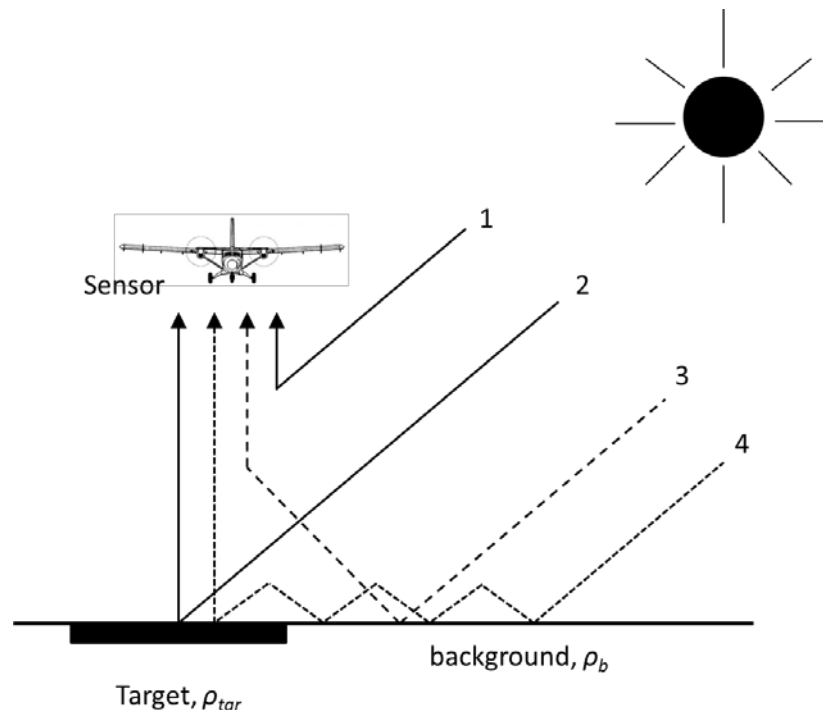


Figure 7. Radiation components contributing to at-sensor radiance. Radiation component 1 represents path radiance and component 2 is the global (diffuse plus direct) solar radiation reflected from the target and transmitted to the sensor. Components 3 and 4 represent the adjacency effect (from Ritter *et. al.* [2006]).

Title: NEON Imaging Spectrometer Radiance to Reflectance Algorithm Theoretical Basis Document		Date: 02/11/2015
NEON Doc. #: NEON.DOC.001288	Author: B. Karpowicz, T. Kampe	Revision: A

The impact on the measured radiance in a given pixel that is due to the adjacency effect is a function of the reflectance contrast between the target pixel and its large-scale neighborhood, and decreases with wavelength (Richter et al., 2006). Correction for the adjacency effect is not part of the standard NEON processing but may be implemented for special cases following quality assessment of flight lines as processing moves from engineering-grade data products to science-grade data products.

To obtain an estimate of the influence of the adjacency effect, a sensitivity analysis using a simple analytical model in conjunction with radiative transfer calculations are presented in Richter et al. [2006]. Two case studies were evaluated as part of this analysis:

- a) A soil target in a dark tar background ( $\rho_{tar}=0.05$ ) with a reflectance contrast of 0.10 in the blue part of the spectrum and a contrast of 0.17 in the 1.6  $\mu\text{m}$  region.
- b) A vegetation target in the same dark tar background with a reflectance contrast of 0.5 in the near-infrared (NIR) region.

The spectral reflectance, as calculated from MODTRAN for each of these surface types used in the simulation, is shown in Figure 8. The MODTRAN simulation takes into account all four of the radiation components identified in Figure 7. Typical clear sky conditions were used in the simulation: solar zenith angle of  $40^\circ$ , a mid-latitude summer atmosphere, rural aerosol, visibility of 23 km, atmospheric water vapor column of 2 cm, ground at sea level, and sensor at 1 m above ground.

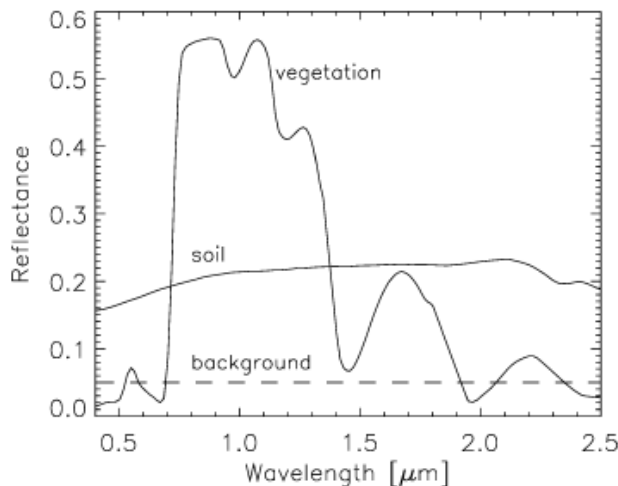


Figure 8. Spectra of vegetation, soil and black tar background used in simulation (from Ritter et al. [2006]).

Title: NEON Imaging Spectrometer Radiance to Reflectance Algorithm Theoretical Basis Document		Date: 02/11/2015
NEON Doc. #: NEON.DOC.001288	Author: B. Karpowicz, T. Kampe	Revision: A

The MODTRAN simulation provides an estimate of the total at-sensor radiance and the path radiance (calculated with ground reflectance set to zero). To obtain results in terms of reflectance, the path radiance was subtracted from the total radiance, the radiance converted to into the equivalent reflectance, and the difference  $\Delta\rho$  of the target to target/background situation computed.

The calculated spectral reflectance difference was then evaluated over a range of sensor-target distances to assess how the measured reflectance was impacted due to reflectance contamination from neighboring pixels. Figure 9 shows the  $\Delta\rho$  curves as a function of sensor-target distance for the soil on dark tar background case. The largest reflectance difference  $\Delta\rho$  occurs in the blue part of the spectrum and decreases with wavelength. At altitudes typical of NEON flights (1 km altitude – 4<sup>th</sup> curve from bottom), a  $\Delta\rho \approx 0.03$  is estimated in the blue portion of the spectrum and decreasing strongly with wavelength. In the 1.6  $\mu\text{m}$  region, the adjacency effect modifies the reflectance by less than  $\Delta\rho = 0.01$  and in the 2.2  $\mu\text{m}$  region by less than  $\Delta\rho = 0.005$ . The reflectance difference is strongly influenced by target-sensor distance: at a wavelength of at 0.400  $\mu\text{m}$  and a target-sensor distance of 1 m,  $\Delta\rho \approx 0.005$ , whereas at a 100-km target-sensor distance  $\Delta\rho \approx$  is 0.05. Thus, the volume scattering (radiation component 3) is a factor of 9 greater than the atmospheric backscattering term (radiation term 4) in this scenario.

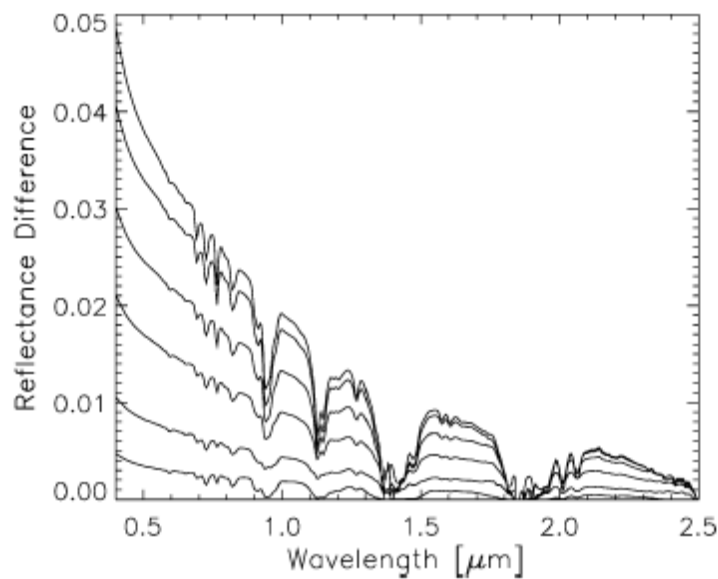


Figure 9. Calculated spectral reflectance difference caused by adjacency effect for soil/tar background case. Curves correspond to sensor altitude. From top to bottom, sensor altitude is 100, 5, 2, 1 and 0.3 km, and 1 m, respectively (from Richter *et al.* [2006]).

Title: NEON Imaging Spectrometer Radiance to Reflectance Algorithm Theoretical Basis Document		Date: 02/11/2015
NEON Doc. #: NEON.DOC.001288	Author: B. Karpowicz, T. Kampe	Revision: A

Figure 10 shows the results for the vegetation on dark tar background case. In this case, only the 0.4-1.0  $\mu\text{m}$  part of the spectrum is shown. This case study can be used to assess the situation where zero reflectance contrast (at wavelengths of 0.53 and 0.58  $\mu\text{m}$ ) and maximum reflectance contrast occur (at 0.8  $\mu\text{m}$ ) – these correspond to situations of no adjacency effect and maximum adjacency effect. The maximum reflectance difference (at 0.8  $\mu\text{m}$ ) is  $\Delta\rho \approx 0.02$  for the shortest sensor-target distance and increases with sensor height to  $\Delta\rho \approx 0.10$  for a 100-km range. At typical NEON flight altitudes (1 km), a reflectance difference  $\Delta\rho \approx 0.05$  is estimated. In the blue part of the spectrum ( $< 0.5 \mu\text{m}$ ) the reflectance difference becomes negative since the reflectance of vegetation is less than the background. At ground level, only the atmospheric backscattering (term 4) is relevant. With increasing sensor altitude, the volume scattering (term 3) becomes dominant. For zero reflectance contrast situations (0.53 and 0.58  $\mu\text{m}$ ), the influence of the adjacency effect vanishes ( $\Delta\rho = 0$ ).

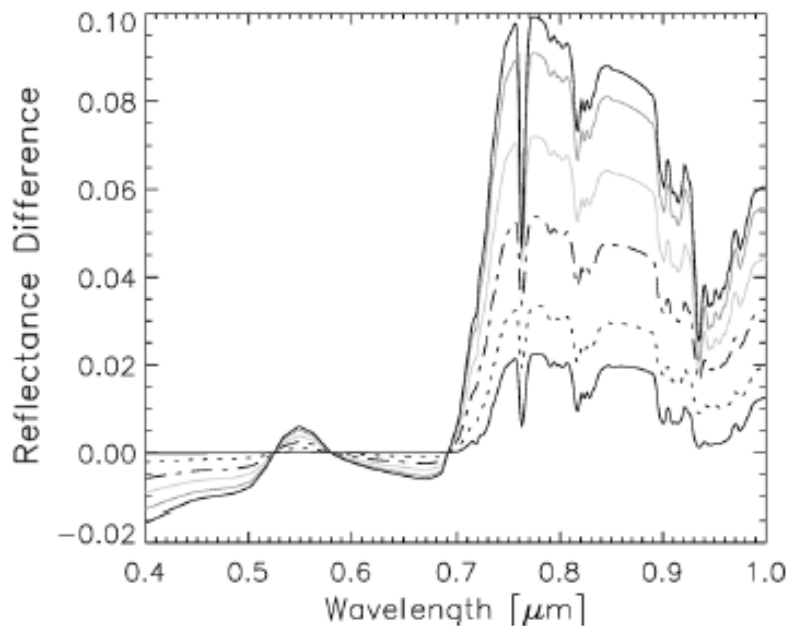


Figure 10. Calculated reflectance difference caused by adjacency effect for vegetation/tar background case. Top to bottom curves at 0.8  $\mu\text{m}$  are sensor at 100, 5, 2, 1, and 0.3 km, and 1 m, respectively (from Richter et. al. [2006]).

Thus, it is apparent that the adjacency effect can introduce erroneous measurements of at-surface radiance. The worst case will occur in scenes containing large reflectance contrasts, such as vegetation near water bodies or regions of extended exposed soil. Based on the analysis

conducted by Richter et al. [2006], it is estimated that at typical NEON flight altitudes, reflectance errors  $\Delta\rho$  as large as 5% can be expected in portions of the spectrum with a large reflectance contrast (e.g., at 0.8  $\mu\text{m}$ ) predominately due to the volume scattering (component 3 of Figure 8) resulting from the adjacency effect.

ATCOR provides an algorithm to correct and remove the spectral contamination due to the adjacency effect and this is described in this section.

The at sensor radiance ( $L$ ) is defined as (Asrar 1989, Chapter 9):

$$L = L_p(\Theta_v, \Theta_s, \phi) + t_v(\Theta_v) \frac{\rho}{\pi} \left( \frac{E_g(0)}{1 - \rho_r s} \right) \quad (32)$$

where  $L_p$  is the path radiance,  $\Theta_v$  is the zenith view angle,  $\Theta_s$  is the solar zenith angle,  $\phi$  is the relative azimuth angle,  $t_v$  is the total ground-to-sensor atmospheric transmittance (sum of direct and diffuse transmittance),  $E_g$  is the global flux on a horizontal surface (sum of direct, and diffuse flux computed with surface reflectance,  $\rho$ , equal to zero),  $\rho_r$  is the large scale reference background reflectance determining the effective global flux (typically,  $\rho_r = 0.15$ ), and  $s$  is the spherical albedo of the atmosphere

The spherical albedo accounts for atmospheric backscattering of radiation to the ground.

The path radiance,  $L_p$ , is defined as

$$L_p(\rho) = L_p(0) + \frac{t_{diff} E_g(0) \left( \frac{\rho}{\pi} \right)}{1 - \rho s} = L_p + t_{diff} E_g(\rho) \left( \frac{\rho}{\pi} \right) \quad (33)$$

$$t_{diff} = \frac{\pi(L_p(\rho_r) - L_p(0))}{\rho_r E_g(\rho_r)} \quad (34)$$

$$E_g(\rho_r) = \frac{E_g(\rho = 0)}{1 - \rho_r s} \quad (35)$$

$$s = \frac{\left[ 1 - \left( \frac{E_g(0)}{E_g(\rho_r)} \right) \right]}{\rho_r} \quad (36)$$

Title: NEON Imaging Spectrometer Radiance to Reflectance Algorithm Theoretical Basis Document		Date: 02/11/2015
NEON Doc. #: NEON.DOC.001288	Author: B. Karpowicz, T. Kampe	Revision: A

In a hyperspectral image, the reflectance  $\rho$  within an individual pixel will differ from the average background reflectance. On a per pixel basis, the observed radiance is composed of 3 parts. The first ( $L_1$ , blue line in Figure 4) is composed of the scattered radiance and the path radiance. The second ( $L_2$ , dark green line in Figure 4) is the radiance received at the sensor as a result of a reflection from the surface pixel. The third ( $L_3$ , the light green line in Figure 4) is the radiation reflected from the neighborhood of the surface pixel and scattered into the viewing direction of the sensor. Only the second component of the observed radiance contains information of the target pixel surface reflectance. It is the third component of the observed radiance that is the contribution due to the adjacency effect.

As a first step in the process, the influence from neighboring pixels are ignored, and the reflectance is computed on a per pixel basis using

$$\rho^{(1)} = \frac{\pi(d^2 L)}{t_v E_g(\rho_r = 0.15)} \quad (37)$$

where  $d$  is the sun-to-earth distance in astronomical units (by definition 1 au is the average distance between the earth and sun). In ATCOR  $d$  is assumed to be 1 au.

The next step is to compute the neighbor average of each pixel in a given range,  $R$  ( $R = 0.5$  to 1 km), defined as

$$\bar{\rho} = \frac{1}{N^2} \sum_{i,j=1}^N \rho_{i,j}^{(1)} \quad (38)$$

where  $N$  corresponds to the number of pixels for a selected range  $R$ . For the range-independent weighting, the adjacency effect is computed as

$$\rho^{(2)}(x, y) = \rho^{(1)}(x, y) + q(\rho^{(1)}(x, y) - \bar{\rho}(x, y)) \quad (39)$$

Where  $q$  indicates the strength of the adjacency effect and is the ratio between the diffuse to direct ground-to-sensor transmittance.

The range dependent version of Equation 39 is written as

$$\rho^{(2)}(x, y) = \rho^{(1)}(x, y) + q \left\{ \rho^{(1)}(x, y) - \int_0^R \rho^{(1)}(r) A(r) \exp(-r/r_s) dr \right\} \quad (40)$$

Title: NEON Imaging Spectrometer Radiance to Reflectance Algorithm Theoretical Basis Document		Date: 02/11/2015
NEON Doc. #: NEON.DOC.001288	Author: B. Karpowicz, T. Kampe	Revision: A

where  $R$  is the range where the intensity of the adjacency effect has dropped to 10%,  $\rho(r)$  is the reflectance at range  $r$  from the  $(x,y)$  position being evaluated, and  $A(r)$  is the area of a circular zone from  $r$  to  $r+dr$ . The discrete form can be written as

$$\rho^{(2)}(x, y) = \rho^{(1)}(x, y) + q \left\{ \rho^{(1)}(x, y) - \sum_{i=1}^{n_R} \bar{\rho}_i w_i \right\} \quad (41)$$

with

$$w_i = \frac{1}{\left( \sum_{i=1}^{n_R} W_i \right)} W_i \quad (42)$$

and

$$W_i = \int_{r_{i-1}}^{r_i} A(r) \exp(-r) dr \approx \int_{r_{i-1}}^{r_i} (2r)^2 \exp(-r) dr \quad (43)$$

ATCOR supports up to  $n_R = 5$  regions. Since the sequence of moving digital low pass filters works with square filters of size  $4r_i^2$ , the area  $A(r)$  is approximated as the corresponding square region  $A(r) = 4r^2$ .

The final step in the ATCOR adjacency correction is to correct for the spherical albedo effect on the global flux that was initially calculated with the reference background of  $\rho_r = 0.15$ . This is the first component of the radiance seen by the pixel as discussed previously and illustrated in Figure 4. The value of 0.15 is an approximation or starting value, and must be updated to reflect the actual neighborhood average of reflectance ( $\bar{\rho}$ ). To do this, the value of  $\rho^{(2)}$  is corrected against the scene-dependent value  $\bar{\rho}$  by correcting with the difference  $\bar{\rho} - \rho_r$ , to yield the final pixel reflectance  $\rho^{(3)}(x,y)$ :

$$\rho^{(3)}(x, y) = \rho^{(2)}(x, y) * \left( 1 - \left( \bar{\rho}(x, y) - \rho_r \right) s \right) \quad (44)$$

### 5.8.2 Atmospheric Correction assuming Rugged Terrain

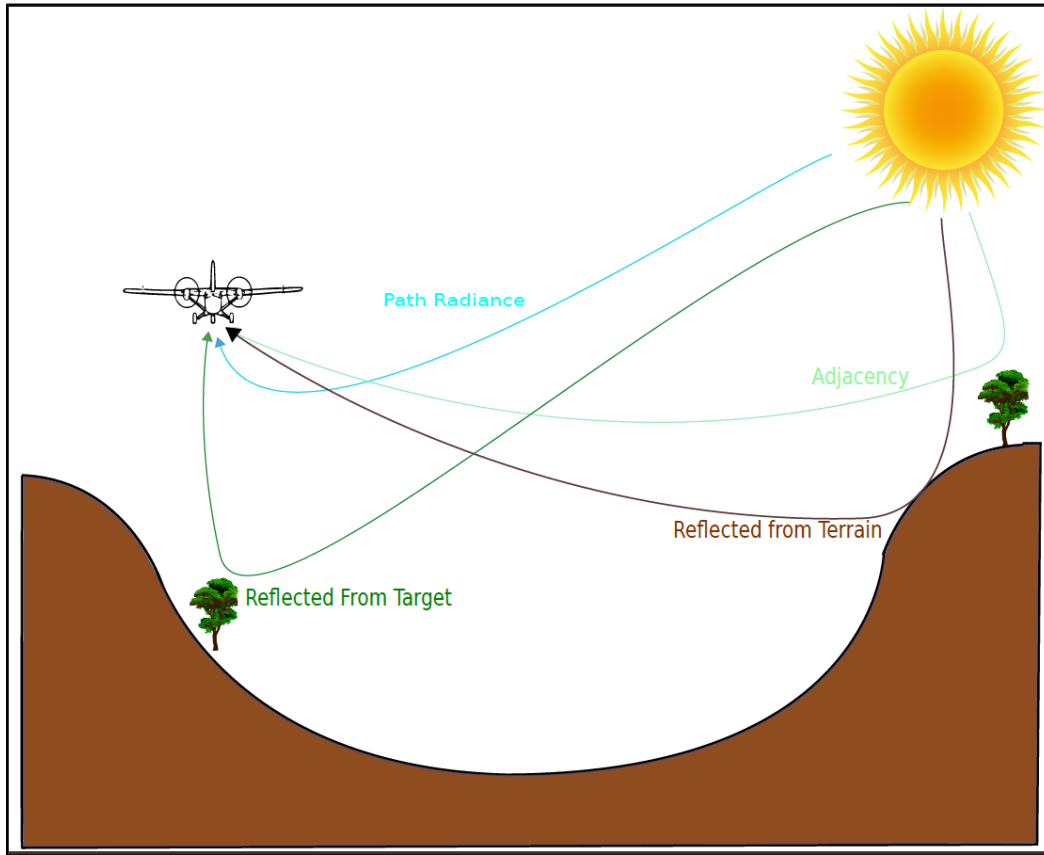


Figure 11: Atmospheric Correction with Rugged Terrain

One of the major challenges in comparing surface reflectance measured by a field spectrometer to the reflectance measured by an airborne system is correcting for changes in illumination resulting from terrain effects. The somewhat simple scenario shown in Figure 4 becomes more complicated as shown in Figure 11 when terrain is considered. The primary challenge then is to correct for surface reflectance in 3 dimensions. The direct and diffuse terms in Equation 25 need to be modified to include terrain geometry and include a neighboring terrain source term. This results in the following iterative equation for computing reflectance (Richter, 1998):

$$\rho^{(i)}(x, y) = \frac{\pi [d^2 L - L_p(z, \theta_v, \phi)]}{t_v(z, \theta_v) [E_{direct}(x, y) + E_{dif}(x, y, z) + E_{terrain}^i(x, y, z)]} \quad (45)$$

Title: NEON Imaging Spectrometer Radiance to Reflectance Algorithm Theoretical Basis Document		Date: 02/11/2015
NEON Doc. #: NEON.DOC.001288	Author: B. Karpowicz, T. Kampe	Revision: A

where  $x$  and  $y$  are the horizontal coordinates,  $z$  is the vertical coordinate,  $L$  is the radiance measured at the sensor,  $L_p(z, \theta_v, \varphi)$  is the path radiance,  $t_v$  is the ground-to-sensor transmittance (direct and diffuse),  $d$  is the earth-sun distance,  $E_{direct}(x, y)$  is the direct radiation incident upon a pixel,  $E_{dif}(x, y, z)$  is the diffuse radiation incident upon a pixel, and  $E_{terrain}^i(x, y, z)$  is the radiation which reflects towards the sensor from the neighboring terrain for iteration  $i$ . Each of the radiation terms in the denominator of Equation 45 are modified to include the effects of terrain. The direct radiation term is modified as

$$E_{direct}(x, y, z) = b(x, y)E_s t_s(z) \cos(\beta(x, y)) \quad (46)$$

where  $b(x, y)$  is a binary flag to indicate whether or not the pixel is directly illuminated,  $E_s$  is the extraterrestrial solar irradiance,  $t_s(z)$  is the sun-to-ground transmittance, and the illumination angle,  $\beta(x, y)$ , is the angle between the direct solar ray and the surface normal and is defined as

$$\cos \beta(x, y) = \cos \Theta_s \cos \Theta_n(x, y) + \sin \Theta_s \sin \Theta_n(x, y) \cos(\phi_s - \phi_n(x, y)) \quad (47)$$

Where  $\Theta_s$  is the solar zenith angle,  $\Theta_n(x, y)$  is the local terrain slope angle,  $\Phi_s$  is the solar azimuth angle, and  $\Phi_n$  is the topographic azimuth angle.

The equation for the diffuse radiation component of Equation 45 is defined as

$$E_{dif}(x, y, z) = E_d(z) \left[ \frac{b(x, y)t_s(z) \cos \beta(x, y)}{\cos \theta_s} + (1 - b(x, y)t_s(z))V_{sky}(x, y) \right] \quad (48)$$

Where  $E_d(z)$  is the diffuse radiation computed by MODTRAN at altitude  $z$ ;  $t_s(z)$  is the sun-to-ground transmittance;  $b(x, y)$  is the binary flag indicating whether the pixel is illuminated by the sun directly ( $b = 1$ ) and  $b = 0$  if shadowed;  $\beta(x, y)$  is the angle between the direct solar ray and surface normal;  $\Theta_s$  is the solar zenith angle; and  $V_{sky}(x, y)$  is the fraction of the sky which is not blocked by terrain (1 for a perfectly flat terrain, and approaching zero for a pixel at the bottom of very narrow valley).  $V_{sky}(x, y)$  is computed using an algorithm described in *Dozier et al. (1981)*.

The final term from Equation 45 is the terrain source term defined as

$$E_{terrain}^i(x, y, z) = E_t^{(i)}(z, \rho_r) \rho_{terrain}^{-(i-1)} V_{terrain}(x, y) \quad (49)$$

Where  $E_t^{(i)}(z, \rho_r)$  is the 0.5 km x 0.5 km box average of the sum of the direct and diffuse radiation at iteration  $i$ ,  $\rho_{terrain}^{-(i-1)}$  is the average reflectance of the terrain at the previous iteration  $i-1$ , and  $V_{terrain}(x, y)$  is the fraction of sky blocked by terrain (i.e.,  $V_{terrain}(x, y) = 1 - V_{sky}(x, y)$ ).

Title: NEON Imaging Spectrometer Radiance to Reflectance Algorithm Theoretical Basis Document		Date: 02/11/2015
NEON Doc. #: NEON.DOC.001288	Author: B. Karpowicz, T. Kampe	Revision: A

For the first iteration a value of 0.1 is used for the average terrain reflectance. While Equation 49 typically converges after three iterations, large values of  $V_{terrain}(x,y)$  or highly reflective surfaces such as snow may require a larger number of iterations.

Following the above steps, the same methodology is used as for a flat surface to account for the adjacency effects (Equations 46, 47, and 51).

## 6 UNCERTAINTY

The uncertainty associated with atmospheric correction is difficult to quantify. The uncertainty will nominally be related to the accuracy of the radiative transfer code used, the accuracy of which aerosols and gaseous constituents of the atmosphere are modeled, the choice of atmospheric input parameters, the terrain type flat vs. rugged, the accuracy of the underlying digital elevation model (DEM), and the reflectance of the surface.

The following table provides an assessment of error contributors for each of the processing steps in the radiance to reflectance processing. The parameters listed in this table will be used to generate an error budget for the radiance to reflectance processing in support of the release of Science-grade Level-1 data products.

It is important to note that many of the contributors listed are wavelength dependent. As an example, as was discussed in the Section 5.8, the impact of the adjacency effect is strongly dependent on the radiance difference between the pixel of interest and the neighboring area. This radiance difference can vary significantly with wavelength depending on the spectral reflectance of the target pixel and background. Similarly, error contributors such as errors in water vapor continuum and aerosol optical depth will have a strong wavelength dependency. This will need to be accounted for in the error budget.

Title: NEON Imaging Spectrometer Radiance to Reflectance Algorithm Theoretical Basis Document		Date: 02/11/2015
NEON Doc. #: NEON.DOC.001288	Author: B. Karpowicz, T. Kampe	Revision: A

Table 6. Initial NIS Radiance to Reflectance Retrieval Error Tree

<u>Processing Step</u>	<u>Contributors</u>
Input data	
Input Radiance File	Spectral calibration error (center wavelength position) [nm] Spectral radiance error [ $\mu\text{W cm}^{-2} \text{sr}^{-1} \text{nm}^{-1}$ ] Spectral response function error (FWHM) [nm] Instrument stray light [ $\mu\text{W cm}^{-2} \text{sr}^{-1} \text{nm}^{-1}$ ]
SBET	Heading error [radians] Flight altitude error [m] GPS time error
Obs file	Path length error [m] Solar zenith angle error [deg] Sensor zenith angle error [deg] Solar azimuth angle error [deg] Sensor azimuth angle error [deg] Phase angle error [deg] Slope/aspect error [deg]

Atmospheric Transmission Calculation (MODTRAN)

	Interpolation error in flight altitude [m] Wavelength interpolation errors [nm] Errors in gaseous species concentrations Error in water vapor continuum
Solar irradiance lookup table	Solar irradiance error [ $\mu\text{W cm}^{-2}$ ]
Aerosol retrieval	Aerosol particle size distribution error Viewing geometry error Path length error Dark target retrieval error Spatial variability in aerosol field
Water vapor retrieval	Spectral calibration error [nm] Water vapor column lookup table error Error in water vapor continuum
BRDF Correction	Solar zenith/azimuth angle errors [deg] Sensor solar/zenith angle errors [deg] Terrain errors (slope, aspect) [deg]
Haze Removal	Error in optical depth Aerosol type error Aerosol size distribution error

Title: NEON Imaging Spectrometer Radiance to Reflectance Algorithm Theoretical Basis Document		Date: 02/11/2015
NEON Doc. #: NEON.DOC.001288	Author: B. Karpowicz, T. Kampe	Revision: A

	Path length error [m]
	Solar zenith/azimuth angle errors [deg]
	Sensor solar/zenith angle errors [deg]
Cloud Shadow Removal	Spectral calibration error (center wavelength) [nm]
	Spectral response function error (FWHM) [nm]
	Spectral radiance error [ $\mu\text{W cm}^{-2} \text{sr}^{-1} \text{nm}^{-1}$ ]
	Spectral response function error (FWHM) [nm]
	Instrument stray light [ $\mu\text{W cm}^{-2} \text{sr}^{-1} \text{nm}^{-1}$ ]
Reflectance Retrieval	Spectral calibration error (center wavelength) [nm]
	Spectral response function error (FWHM) [nm]
	Spectral radiance error [ $\mu\text{W cm}^{-2} \text{sr}^{-1} \text{nm}^{-1}$ ]
	Spectral response function error (FWHM) [nm]
	Instrument stray light [ $\mu\text{W cm}^{-2} \text{sr}^{-1} \text{nm}^{-1}$ ]
Adjacency effect	Radiance error due to adjacency effect [ $\mu\text{W cm}^{-2} \text{sr}^{-1} \text{nm}^{-1}$ ]
Terrain compensation	Solar zenith/azimuth angle errors [deg]
	Sensor solar/zenith angle errors [deg]
	Terrain errors (slope, aspect) [deg]

## 6.1 Analysis of Uncertainty

Ultimately, a thorough analysis of uncertainty will need to be performed using ground-truth measurements along with a radiative transfer model which has more transparency than the lookup tables generated for ATCOR. Previous analysis using ATCOR has resulted in an estimated accuracy of +/-2% for a retrieved reflectance < 10%, and an accuracy of +/-4% for a retrieved reflectance of > 40% (ER [03]). It should be noted, however, that these accuracies were achieved by avoiding specular reflection and areas of flat terrain. It was found in *Richter* (1998) that errors exceeding 100% may occur for certain geometries such as a mountain ridge with a half-pixel offset between the imagery and the DEM.

## 6.2 Reported uncertainty

The underlying algorithms, and databases for ATCOR are currently a black box, and it is not possible to report an uncertainty at this time. Excluding extreme cases, the error in reflectance will likely be in the 5-10 % range outside of strong water vapor, and CO<sub>2</sub> absorption bands.

Title: NEON Imaging Spectrometer Radiance to Reflectance Algorithm Theoretical Basis Document		Date: 02/11/2015
NEON Doc. #: NEON.DOC.001288	Author: B. Karpowicz, T. Kampe	Revision: A

## 7 VALIDATION AND VERIFICATION

The validation and verification of the algorithm will take place over a number of sites where ground-truth measurements are available. Each year a calibration flight over a well-characterized site with simultaneous field spectrometer data will be taken as described in the NIS calibration plan (RD [08]). The surface reflectance taken with field spectrometers will be compared with the NIS data to validate the atmospheric correction algorithm. Retrieval of aerosol optical depth by sunphotometers deployed by AOP and located at tower sites may be used as a spot check of the ATCOR retrieved aerosol optical depth.

## 8 FUTURE MODIFICATIONS AND PLANS

NEON is currently investigating incorporating measurements of downwelling and upwelling radiance collected simultaneously with the imaging spectrometer into the atmospheric correction algorithm. It is expected that these measurements should provide additional information to constrain the atmospheric constituents in real time which will improve the representation of aerosols and water vapor in the radiative transfer model underlying the atmospheric correction algorithm.

As discussed in Section 7, the analysis of uncertainty and error assessment associated with this algorithm will be refined as these data products are matured from Engineering-Grade to Science-Grade. As part of this effort, it will be necessary to quantify uncertainties due to the instrument, atmospheric, and geometric variables, as well as contributions due to algorithmic processing steps/decisions. This will require comparisons of retrievals against ground-truth (tarps) and field measurements (ASD field spectrometer) that will be conducted as part of upcoming AOP flight campaigns. The AOP team is also evaluating the feasibility of incorporating data from spectral irradiance monitors flown on-board the AOP platform that will acquire downwelling and upwelling irradiance measurements acquired coincidentally with the imaging spectrometer data that should provide significantly improve real time estimates of the atmosphere to better constrain estimates aerosols, water vapor, and visibility.

## 9 BIBLIOGRAPHY

Adler-Golden, S. M., M. W. Matthew, G. P. Anderson, G. W. Felde, and J. A. Gardner (2002), An Algorithm for De-Shadowing Spectral Imagery, in *Airborne Earth Science Workshop, 5-8 March 2002, JPL-Publication 03-04*, vol. 01803, Pasadena, U.S.A.

Asrar, G., "Theory and Applications of Optical Remote Sensing", J. Wiley, New York, (1989).

Title: NEON Imaging Spectrometer Radiance to Reflectance Algorithm Theoretical Basis Document		Date: 02/11/2015
NEON Doc. #: NEON.DOC.001288	Author: B. Karpowicz, T. Kampe	Revision: A

Crist, E. P., and R. C. Cicone (1984), A Physically-Based Transformation of Thematic Mapper Data—The TM Tasseled Cap, *IEEE Transactions on Geoscience and Remote Sensing*, GE-22(3), 256–263, 10.1109/TGRS.1984.350619.

Dozier, J., J. Bruno, and P. Downey (1981), A faster solution to the horizon problem, *Computers & Geosciences*, 7, 145–151.

Fontenla, J. M., J. Harder, W. Livingston, M. Snow, and T. Woods (2011), High-resolution solar spectral irradiance from extreme ultraviolet to far infrared, *Journal of Geophysical Research*, 116(D20), D20,108, 10.1029/2011JD016032.

Kaufman, Y., A.E. Wald, L. Remer, and L. Flynn (1997), The MODIS 2.1-um channel-correlation with visible reflectance for use in remote sensing of aerosol, *IEEE Transactions on Geoscience and Remote Sensing*, 35(5), 1286–1298, 10.1109/36.628795.

Kurucz, R. L. (2005), The solar irradiance by computation, <http://cfaku5.cfa.harvard.edu/papers/irradiance/>.

Richter, R. (1996), Atmospheric correction of satellite data with haze removal including a haze/clear transition region, *Computers & Geosciences*, 22(6), 675–681, doi: 10.1016/0098-3004(96)00010-6. Richter, R., (1998), Correction of satellite imagery over mountainous terrain, *Applied Optics*, 37(18), 4004-4015, doi: 10.1364/AO.37.004004

Richter, R., and D. Schläpfer (2002), International Journal of Geo-atmospheric processing of airborne imaging spectrometry data . Part 2 : Atmospheric / topographic correction, *International Journal of Remote Sensing*, 23(23:13), 2631–2649.

Richter, R., and A. Müller (2005), De-shadowing of satellite/airborne imagery, *International Journal of Remote Sensing*, 26(15), 3137–3148, doi: 10.1080/01431160500114664.

Richter, R., Bachmann, M., Dorigo, W., Mueller, A. (2006), Influence of the adjacency effect on ground reflectance measurements, *IEEE Geoscience Remote Sensing Letters*, Vol. 3, 565-569.

Richter, R., and D. Schlapfer (2008), Considerations on water vapor and surface reflectance retrievals for a spaceborne imaging spectrometer, *IEEE Transactions on Geoscience and Remote Sensing*, 46(7), 1958–1966, doi: 10.1109/TGRS.2008.916470.

Richter, R., and D. Schläpfer (2011), Atmospheric/topographic correction for airborne imagery (ATCOR-4 User Guide, Version 6.0.2), *Tech. Rep. August*, DLR, Wessling, Germany.

Title: NEON Imaging Spectrometer Radiance to Reflectance Algorithm Theoretical Basis Document		Date: 02/11/2015
NEON Doc. #: NEON.DOC.001288	Author: B. Karpowicz, T. Kampe	Revision: A

Schläpfer, D., J. Keller, and K. I. Itten (1996), Imaging spectroscopy of tropospheric ozone and water vapor, in *15th EARSeL Symposium*, pp. 439–446.

Schläpfer, D., C. Borel, J. Keller, and K. Itten (1998), Atmospheric precorrected differential absorption technique to retrieve columnar water vapor, *Remote Sensing of Environment*, 65, 353–366.

Van de Hulst, H. C. (1957), *Light Scattering by Small Particles*, Wiley, New York, New York.

Yi, C. (2008), Haze reduction from the visible bands of LANDSAT TM and ETM+ images over a shallow water reef environment, *Remote Sensing of Environment*, 112(4), 1773–1783, doi: 10.1016/j.rse.2007.09.006.

Zhang, Y., B. Guindon, and J. Cihlar (2002), An image transform to characterize and compensate for spatial variations in thin cloud contamination of Landsat images, *Remote Sensing of Environment*, 82(2-3), 173–187, doi: 10.1016/S0034-4257(02)00034-2.